remote sensing

MDPI

Review

Lunar Mare Fecunditatis: A Science-Rich Region and a Concept Mission for Long-Distance Exploration

Siyuan Zhao [1], Yuqi Qian [1], Long Xiao [1,*], Jiannan Zhao [1], Qi He [1], Jun Huang [1], Jiang Wang [1], Hui Chen [2] and Weiyang Xu [2]

[1] State Key Laboratory of Geological Processes and Mineral Resources, Planetary Science Institute, School of Earth Sciences, China University of Geosciences, Wuhan 430074, China; siyuanzhao@cug.edu.cn (S.Z.); yuqi_qian@cug.edu.cn (Y.Q.); jnzhao@cug.edu.cn (J.Z.); he_qi@cug.edu.cn (Q.H.); junhuang@cug.edu.cn (J.H.); j.wang@cug.edu.cn (J.W.)

[2] Aerospace System Engineering Shanghai, Shanghai 201109, China; 13761181357@163.com (H.C.); weiyang.xu@outlook.com (W.X.)

* Correspondence: longxiao@cug.edu.cn

Abstract: Mare Fecunditatis is a ~310,000 km^2 flat basalt plain located in the low-latitude area of the Moon. Plenty of volcanic features (multiple episodes of mare basalts, sinuous rilles, lava tubes, pyroclastic deposits, domes, irregular mare patches (IMP), ring-moat dome structures (RMDS), floor-fractured craters), tectonic features (grabens and wrinkle ridges), impact-related features, and other features (swirls, pit craters) are identified in Mare Fecunditatis. An in-situ mission to Mare Fecunditatis is scientifically significant to better understand the lunar thermal histories and other questions. All previous in-situ and human missions (Apollo, Luna, Chang'E) were limited to small areas, and no traverse longer than 40 km has been made yet. With the development of technology, long-distance movement will be possible in the future on the lunar surface, providing opportunities to explore multiple sites at one mission with complete documentation of the regional geology. Eight high-value targets (pit crater, IMPs, RMDSs, young basalts, high-Al basalts, pyroclastic deposits, swirls, and fresh craters) were found in Mare Fecunditatis, and a ~1400 km-traverse in 5 years is proposed to explore them to solve the most fundamental lunar questions.

Keywords: Moon; Mare Fecunditatis; long-distance exploration

Citation: Zhao, S.; Qian, Y.; Xiao, L.; Zhao, J.; He, Q.; Huang, J.; Wang, J.; Chen, H.; Xu, W. Lunar Mare Fecunditatis: A Science-Rich Region and a Concept Mission for Long-Distance Exploration. *Remote Sens.* **2022**, *14*, 1062. https://doi.org/10.3390/rs14051062

Academic Editor: Akira Iwasaki

Received: 8 January 2022
Accepted: 18 February 2022
Published: 22 February 2022

1. Introduction

The Soviet Union, United States, Europe, China, Japan, and India have successively conducted their lunar robotic or crewed missions since the 1960s. Extraordinary scientific discoveries have been made, but even more questions have been proposed, including (1) bombardment history, (2) lunar interior, (3) crust and regolith, (4) polar region and volatiles, (5) volcanism and thermal evolution, (6) impact process, and (7) space weathering [1], and more scientific landing sites across the Moon have been proposed (e.g., [2–7]). However, different high-value targets are distributed all over the Moon and are normally far away from each other (Figure 1). The short detection distance (less than 39 km, made by Lunokhod 2 in 1973) of previous missions limited the complete scientific documentation of the investigation area, and exploring multiple sites in large distance at one mission was impossible in the era. With the development of technologies, multi-target long-distance missions [8,9] in the near future may become reality. The Intrepid mission [8] concept is one of the examples. The designed rover plans to travel ~1800 km in the Oceanus Procellarum in a 4-year period, which will explore Reiner Gamma, Marius Hills, young mare basalts, Aristarchus Plateau, Aristarchus Crater, and irregular mare patches (IMPs). Both 4 and 1.2 billion years of volcanic activity on the Moon could be revealed by Intrepid.

The long travel distance would make the scientific outcomes several times larger than a normal rover mission.

Mare Fecunditatis (centered at 7.8°S, 53.7°E) is a low-latitude area with flat terrain on the nearside of the Moon. The basin formed in the pre-Nectarian period (>3.92 Ga), while the mare basalts were mainly filled in the Imbrian period (3.2–3.85 Ga) and continued until the Eratosthenian period (1.1–3.2 Ga) [10–12]. There is a diversity of volcanic features (e.g., mare deposits, sinuous rilles, lava tubes, pyroclastic deposits, domes, irregular mare patches, ring-moat dome structures), tectonic features (e.g., graben and wrinkled ridge), impact-related features, and other features (e.g., swirls, pit craters) in Mare Fecunditatis. A composite of in-situ investigations of these features will provide a window to understand the external and internal processes. In this study, the scientific value of eight targets (pit crater, IMPs, RMDSs, young basalts, high-Al basalts, pyroclastic deposits, swirls, and fresh craters) was listed, and a ~1400 km traverse routine through Mare Fecunditatis in 5 years was proposed, which would help the planning of long-distance missions in the future.

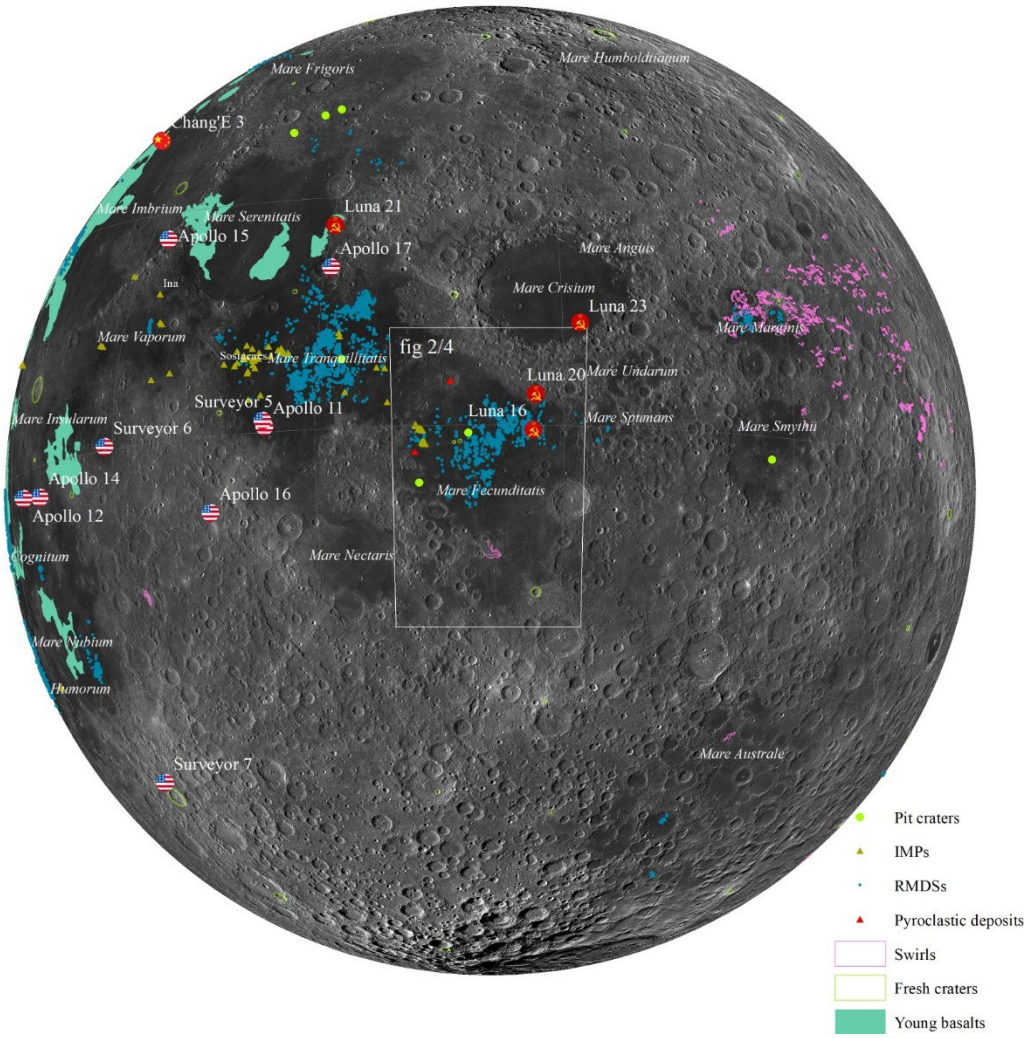

Figure 1. Orthographic map of Wide Angle Camera (WAC, [13]) image with projection center in Mare Fecunditatis (7.8°S, 53.7°E). The flag icons stand for the previous soft-landing missions of the United States, Soviet Union, and China, respectively. The green points, dark yellow triangles, blue points, red triangles, pink outlines, green outlines, and jadeite areas represent identified pit craters [14], IMPs [15], RMDSs [16], pyroclastic deposits [17,18], swirls [19], fresh craters [20], and young basalts (≤3.0 Ga, [21–25]), respectively. The white box represents the locations of other figures in this paper.

2. Topography of Mare Fecunditatis

Mare Fecunditatis is located in the low-latitude area on the eastern nearside of the Moon, covering an area of ~310,000 km² (Figures 1 and 2a). SELENE and LRO DEM 2015 (SLDEM2015, 60 m/pixel, [26]) data show that Mare Fecunditatis has a higher elevation in the southwest and a lower elevation in the northeast, and the elevation of 99% of Mare Fecunditatis varies from −0.3 km to −2.7 km (Figure 2b). The peak ring of the Mare Fecunditatis basin is strongly degraded, and the outline is difficult to distinguish [27]. The slope in the basin interior is relatively gentle (average slope of 3.56°); more than 99% of the area has a slope of less than 20°, and 84% of the area has a slope of less than 5° (Figure 2c). Roughness [28] based on the median slope of the 57 m-baseline Lunar Orbiter Laser Altimeter (LOLA, [29,30]) data shows an average value is 1.7°, while the roughness of more than 90% of the area is less than 2.6° (Figure 2d). Mare Fecunditatis is relatively flat, and only crater rims appear with large roughness.

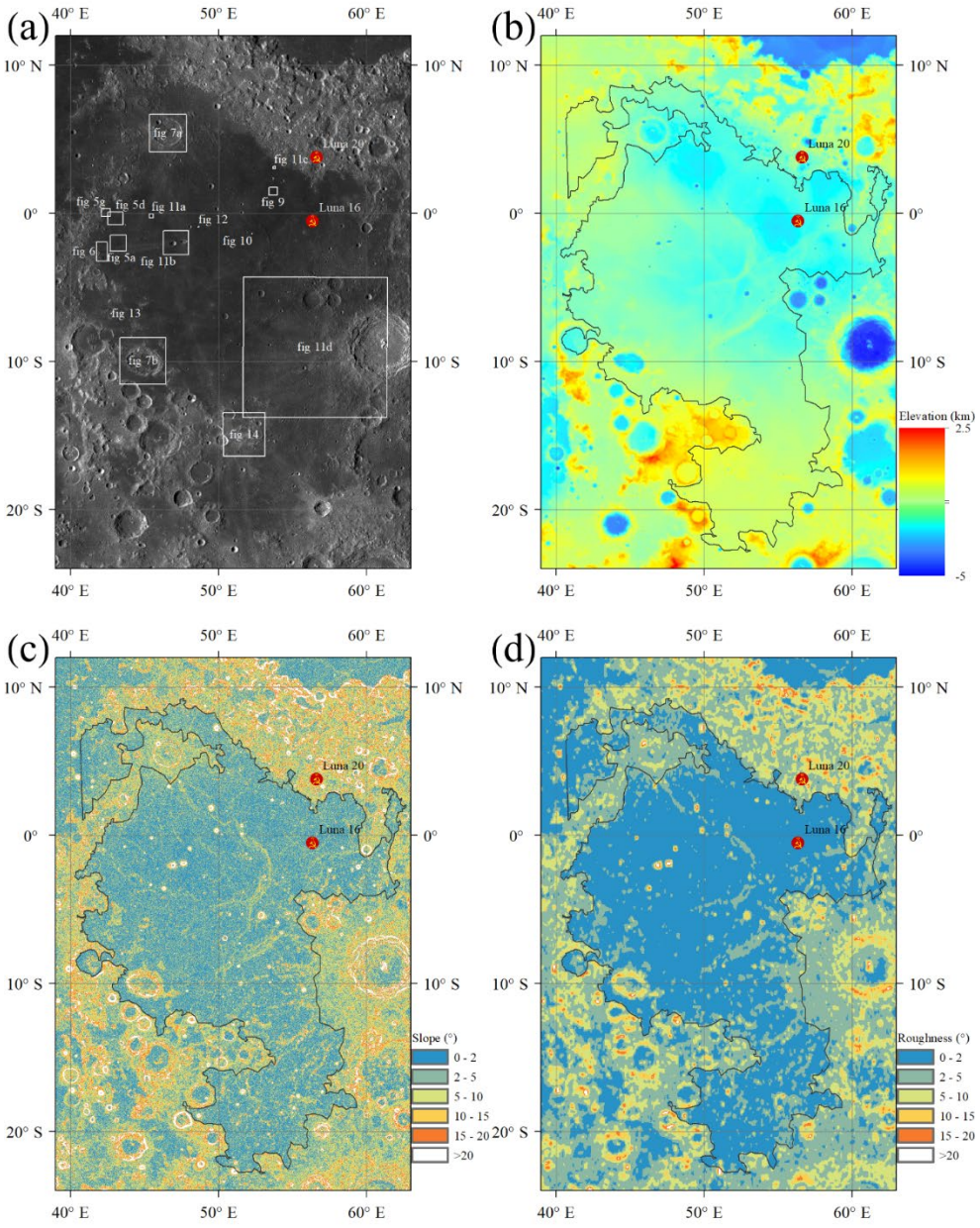

Figure 2. The (**a**) WAC image. The white boxes represent the locations of other figures in this paper (**b**) SLDEM2015, (**c**) SLDEM2015 slope, and (**d**) LOLA roughness of Mare Fecunditatis.

3. Geology and Geomorphology of Mare Fecunditatis

Mare Fecunditatis basin was formed in the pre-Nectarian period, followed by the mare basalts eruption in the Imbrian period, and the volcanic activity continued until the early Eratosthenian period [10–12]. There is no mass concentration in the center of Mare Fecunditatis [31], while there are positive Bouguer anomalies on the east and west sides [32] of the basin. A diversity of geological features (Figure 3) is found in Mare Fecunditatis.

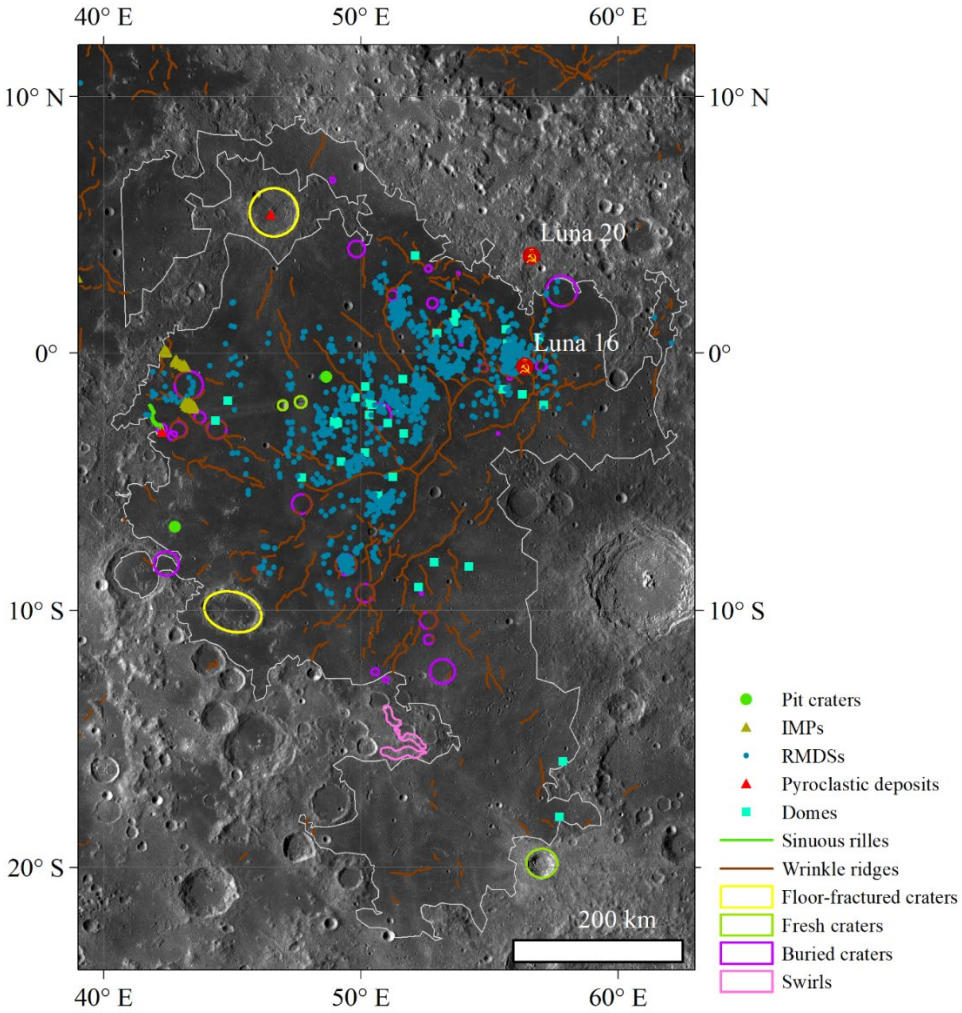

Figure 3. Geological features in Mare Fecunditatis, shown with a WAC image. The green points, dark yellow triangles, blue points, red triangles, bluish green boxes, green lines, brown lines, yellow outlines, green outlines, purple outlines, and pink outlines represent identified pit craters [14], IMPs (updated from [15]), RMDSs [16], pyroclastic deposits [17,18], domes, sinuous rilles [33], wrinkle ridges [34], floor-fractured craters [35], fresh craters [20], buried craters, and swirls [19], respectively.

3.1. Volcanic Features

3.1.1. Mare Basalts

Lunar mare basalt is the main volcanic product of lunar mare volcanism, originated from the partial melting of the lunar mantle and filling some of the impact basins after eruption, including Fecunditatis basin, forming Mare Fecunditatis.

The basalt in Mare Fecunditatis has an average thickness of ~500 m [36], with a thickness of up to 1500 m in the center [37]. The Multiband Imager (MI, [38]) FeO map shows that Mare Fecunditatis is 17–20 wt% in the center and 14–17 wt% in the south (Figure 2a, [39,40]). The WAC TiO_2 map [41] shows high-Ti (TiO_2 > 6 wt%) and low-Ti (TiO_2: 2–6 wt%) basalts are mainly distributed in the center of the basin, while very low-Ti (TiO_2 < 2 wt%)

basalts are mainly distributed in the and southern region (Figure 2b). Interference Imaging Spectrometer (IIM, [42,43]) Al maps [44] show high-Al (Al_2O_3 > 11 wt%) basalts are widely distributed in the Mare Fecunditatis, except for the northeastern part; the results are similar with the compositional constraints based on FeO, TiO_2, and Th maps [45,46].

Luna 16 landed in the northeastern part of Mare Fecunditatis (0.7°S, 56.3°E) in 1970. All returned basalt fragments have high-Al (Al_2O_3 > 11 wt%) characteristics [47], with a TiO_2 content of 1–5 wt%, Al_2O_3 content of 11–20 wt%, and Mg# (Mg/(Mg+Fe) in mole percent) of 0.3–0.4 [47,48]. The isotopic ages of basalt samples show three-episode magmatic activities between ~3.14 and 3.42 Ga, but concentrate in ~3.4 Ga [49–52]. According to the mare unit map [12] (Figure 4d), the age of the unit where Luna 16 landed is 3.36 Ga, which is in good agreement with the 3.4 Ga isotopic age. The age of the low-Ti, high-Al basalt in the central and southern parts is 3.5–3.7 Ga, while the high-Ti basalt in the northeast is relatively young, at 3.34–3.36 Ga, and the magmatic activity of some basalts in the southwest continues to 3.14 Ga. In addition, we find a small number of areas with lower albedo, fewer craters, and fewer ejecta materials. Among them, three areas show relatively younger ages (2.2–2.9 Ga; Figure 5).

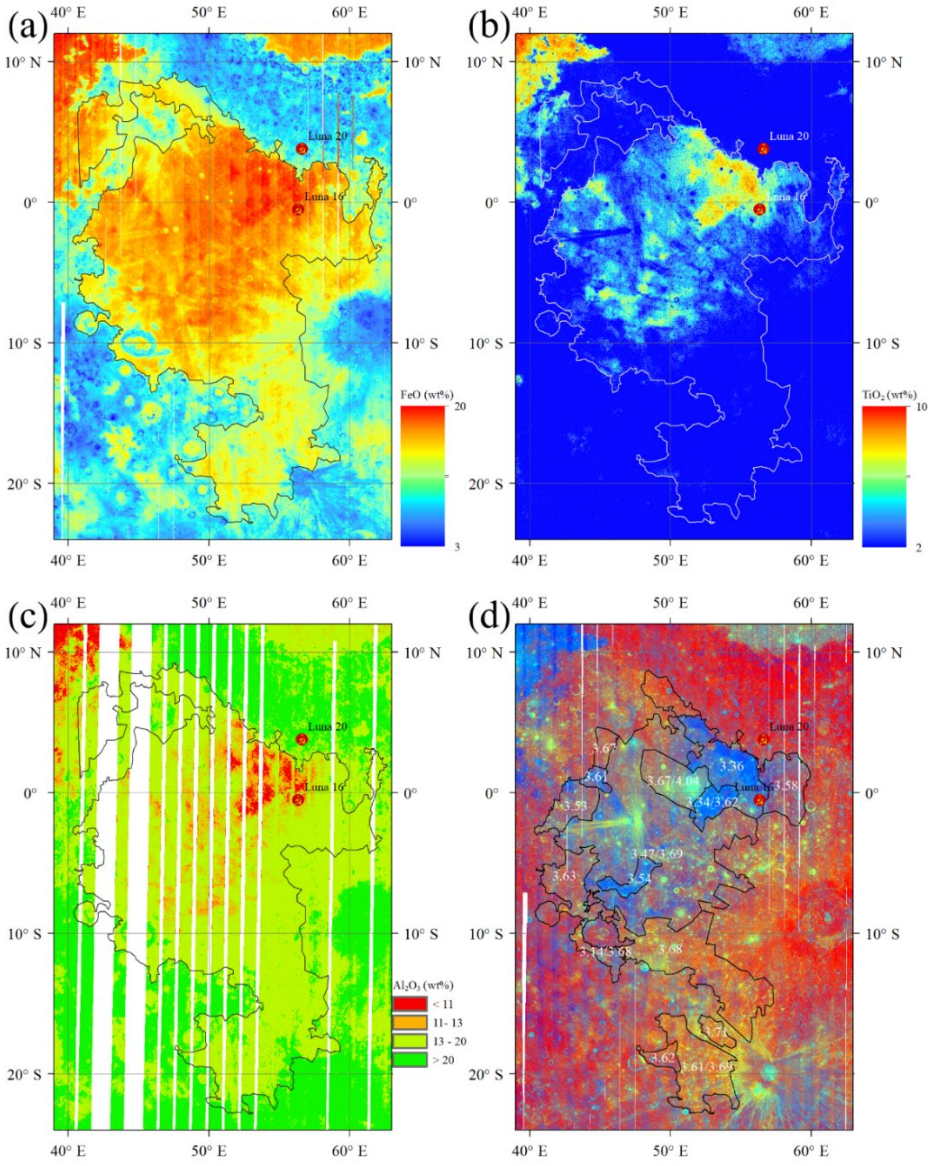

Figure 4. The (**a**) MI FeO map, (**b**) WAC TiO_2 map, (**c**) IIM Al_2O_3 map, and (**d**) MI color ratio map and the age of different geological units (adapted from [12]) of Mare Fecunditatis.

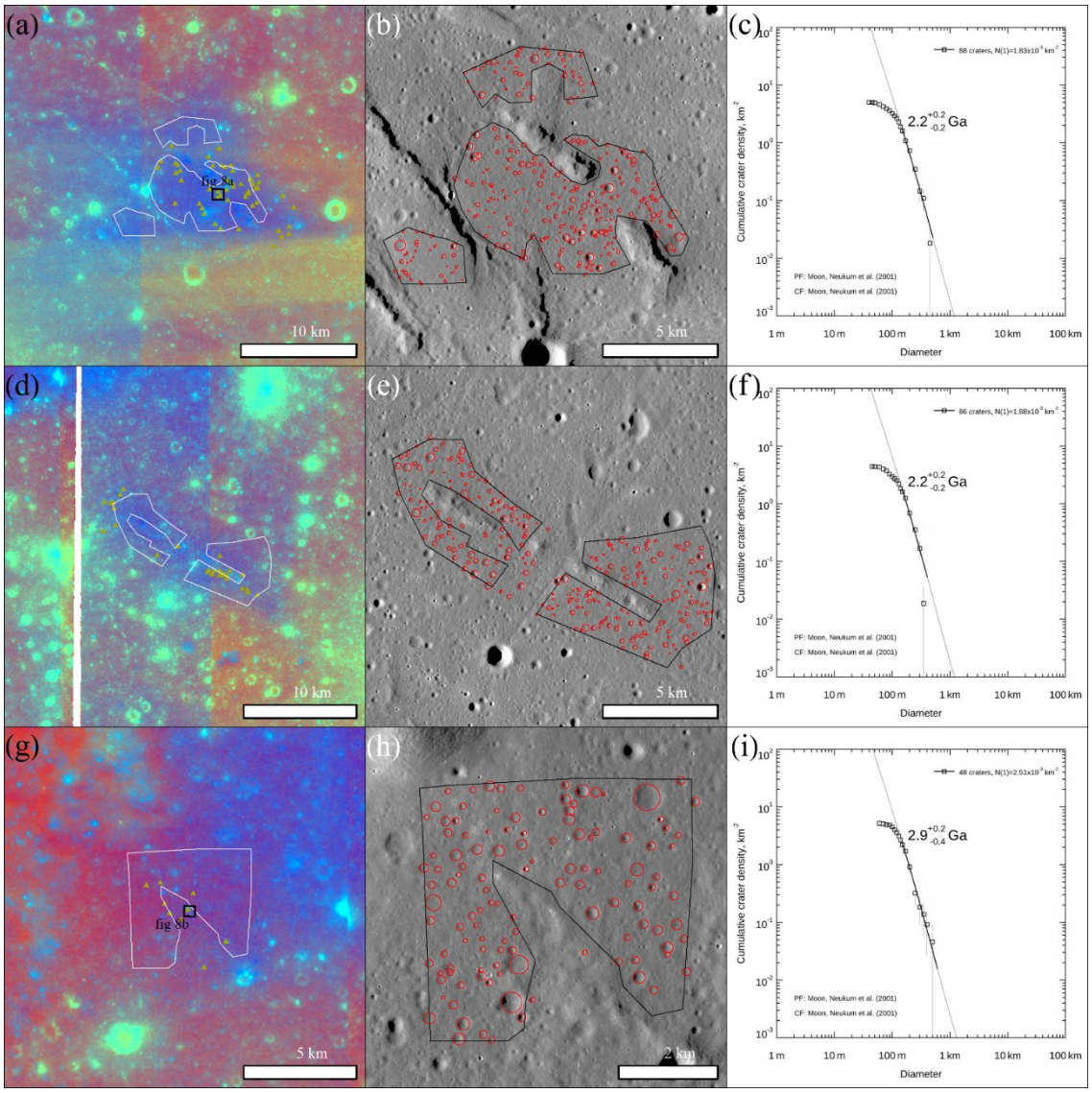

Figure 5. Crater size–frequency distribution measurements of three Eratosthenian-aged basalt areas with IMPs (dark yellow triangles); craters with diameter > 150 m are used for dating. (**a**) MI color ratio map of counting area 1 (2.0°S, 43.2°E); (**b**) crater counting of area 1, shown with a Terrain Camera (TC, [53]) image; (**c**) absolute model age of area 1; (**d**) MI color ratio map of counting area 2 (0.4°S, 43.0°E); (**e**) crater counting of area 2, shown with a TC image; (**f**) absolute model age of area 2; (**g**) MI color ratio map of counting area 3 (0.1°N, 42.4°E); (**h**) crater counting of area 3, shown with a TC image; (**i**) absolute model age of area 3. The black boxes represent the locations of other figures in this paper.

3.1.2. Sinuous Rilles

Sinuous rilles are formed by the erosion of the lunar surface or the continuous collapse of lava tubes during the flow of high-temperature lava, which usually originates from a depression, extending from high terrain to low terrain, and gradually disappears on the smooth lunar mare [54]. A short small-scale sinuous rille (Figures 3 and 6) is found in the western part of Mare Fecunditatis, adjacent to pyroclastic deposits. This sinuous rille is 26.8 km in length, 1000 m wide, and 69 m deep. A possible 17.5 km long collapsed lava tube with 0.69 km in width and 65 m in depth is also discovered next to the sinuous rille.

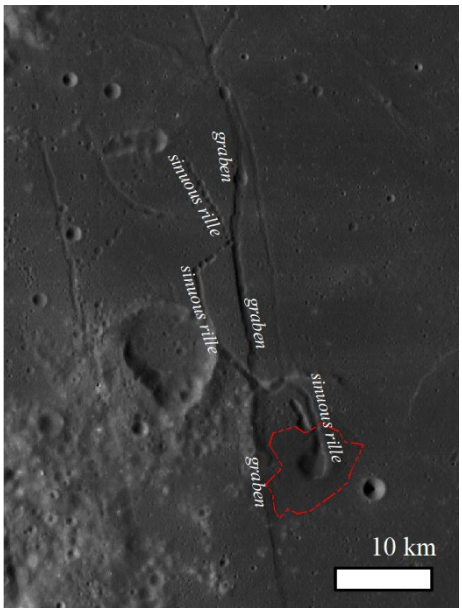

Figure 6. Sinuous rille, graben, and pyroclastic deposits (red dotted outline) in western Mare Fecunditatis (2.5°S, 42.0°E), shown with a WAC image.

3.1.3. Floor-Fractured Craters

The Taruntius crater (5.5°N, 46.5°E, Figure 7a) and Goclenius crater (10.0°S, 45.0°E, Figure 7b) are found in the northern and western part of the Mare Fecunditatis, respectively. Their floors are cut by concentric or polygonal fractures, known as floor-fractured craters (FFCs) [35,55,56]. There are two formation hypotheses for FFCs: (1) viscous relaxation, wherein the crater floor rebounds to fill the crater at a rate controlled by the subsurface viscosity structure, resulting in an overall amplitude shallowing of long-wavelength crater topography [57]; and (2) magma intrusions and sills form beneath the crater, and the magma lifting produces the laccolith and fractures the overlying the crater floor [35,55,56,58]. Recent numerical simulations do not support the viscous relaxation hypothesis [59], but high-resolution topographic and gravity data advocate the magma intrusion hypothesis [35,55,56].

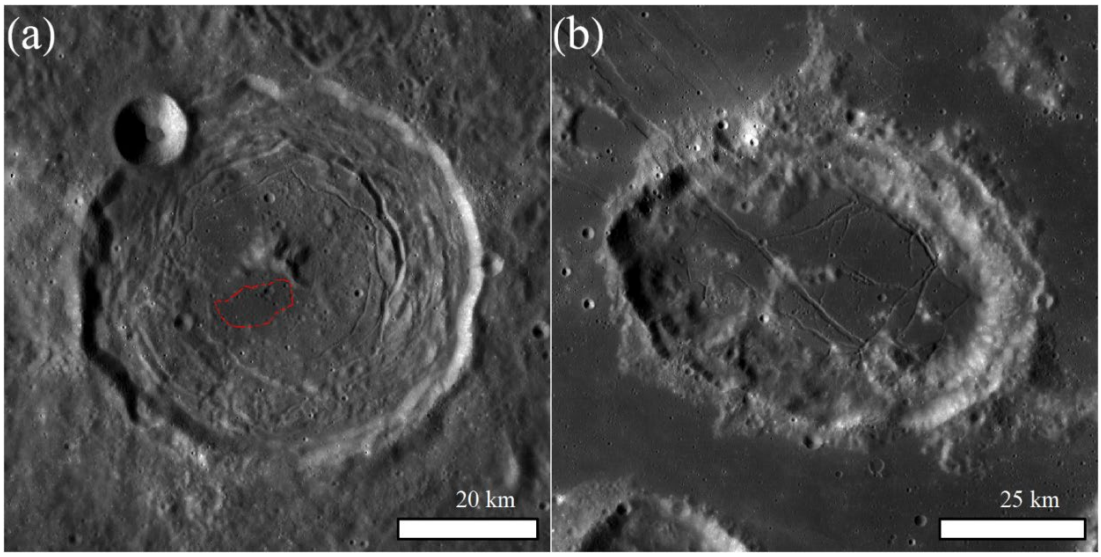

Figure 7. Floor-fractured craters, shown with WAC images. (**a**) Crater Taruntius (5.5°N, 46.5°E) with dark mantle pyroclastic deposits in the center (red dotted line); (**b**) Crater Goclenius (10.0°S, 45.0°E).

3.1.4. Pyroclastic Deposits

Pyroclastic deposits are the products of explosive volcanism, and the characteristic richness in glass and titanium make them darker than overflow basalts [60]. They have a smooth surface and usually occur close to sinuous rilles, irregular depressions, and the boundary between the maria and highlands [61]. Two areas in Mare Fecunditatis have pyroclastic deposits: in the Taruntius crater [62] on the northern side of the center peak (Figure 7a, 5.4°N, 46.5°E), and the area connecting to the sinuous rille (Figure 6, 3.0°S, 42.3°E).

3.1.5. Irregular Mare Patches

Irregular Mare Patches (IMPs) are enigmatic features occurring in the lunar mare. Typical IMPs (such as Ina (18.65°N, 5.30°E) and Sosigenes (8.335°N, 19.071°E), Figure 1) are one to several kilometers in size and composed of positive-relief mounds surrounding low rough hummocky and/or blocky floor units. The IMPs in Mare Fecunditatis are relatively small (tens to hundreds of meters in size) and only develop irregular, rough, bright, and pit features. They may be formed by (1) sublimation [63]; (2) small magma intrusion on the top of the dome [64–66]; (3) clearing of the overlying lunar regolith by outgassing activity within 10 Ma [67]; (4) lava flow inflation [68]; (5) basalt eruption within 100 Ma [15]; (6) pyroclastic eruption [69]; and (7) lava lake process and foamy magma extrusion [70–73]. The most fundamental scientific question of IMP is whether they are young or not. Some authors [15] suggest that IMPs have ages younger than 100 Ma based on impact crater chronologies. Others proposed IMP formed contemporarily with the Imbrian-aged host basalts [68,70].

In the western part of Mare Fecunditatis, dozens of IMPs (Figure 3) are identified within a length of tens to hundreds of meters. They are distributed on three small Eratosthenian-aged areas (Figure 5), where TiO_2 content is > 4 wt%. Most of the IMPs are located next to the rim of craters (Figure 8a), and a few IMPs are not connected to the crater (Figure 8b).

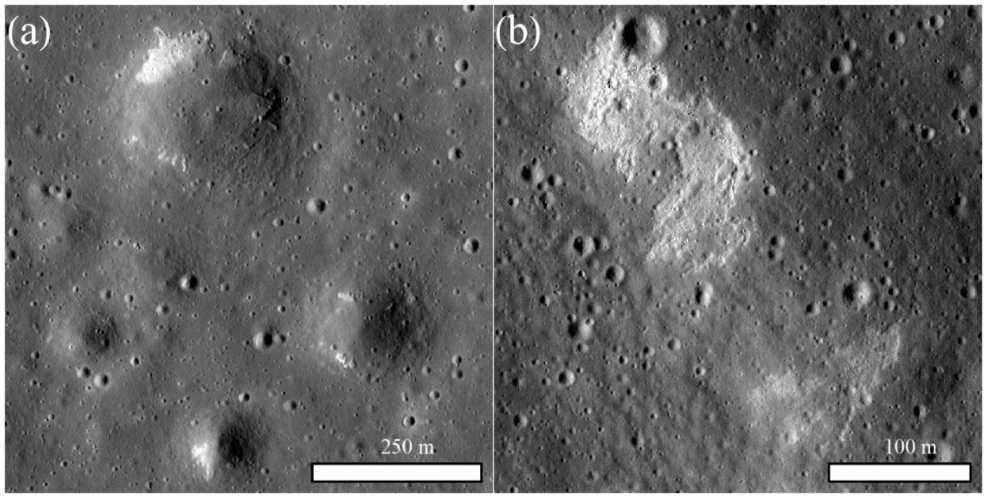

Figure 8. Two sites of IMP in Mare Fecunditatis, shown with Narrow Angle Camera (NAC, [13]) images. (**a**) IMPs next to the crater rim (2.02°S, 43.31°E); (**b**) IMPs on the mare (0.09°N, 42.41°E). Data source: NAC M1230441915RE and NAC M150239673LE.

3.1.6. Domes

The lunar volcanic domes are formed by (1) cooling limited lava flows [74]; (2) subsurface intrusion [75]; and combination of (2) and (1) [76]. There are at least 38 domes (e.g., Figure 9) with a diameter of more than 500 m in the Mare Fecunditatis, mainly distributed in the center of Fecunditatis where the content of TiO_2 generally exceeds 3 wt%.

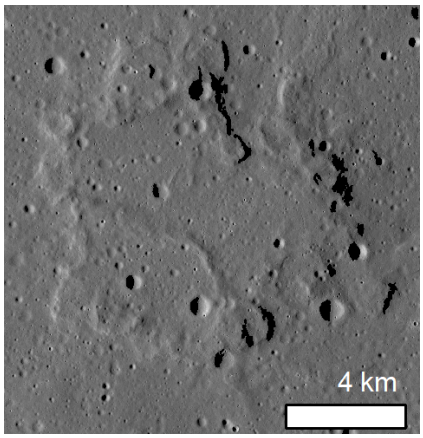

Figure 9. The largest dome (1.5°N, 53.7°E) in Mare Fecunditatis, shown with a TC image.

3.1.7. Ring-Moat Dome Structures

RMDS is a newly discovered lunar volcanic feature [77]. RMDSs are small circular mounds hundreds of meters in diameter and ~3–4 m in height, surrounded by narrow, shallow moats (Figure 10). Four hypotheses were proposed for the formation of RMDSs [77]: (1) high-viscous lava eruption soon after the mare basalt; (2) geologically very recent eruption; (3) small-scale squeezing features formed at the time of the mare basalt; and (4) volatility-rich magmatic foam extrusion. More than 1,600 RMDSs have been identified in the Mare Fecunditatis [16] and they are concentrated in the northern sector, where TiO_2 contents of the RMDS-bearing basalt are larger than 3 wt% and absolute model ages range from 3.36 to 3.67 Ga [12]. The height of RMDSs is very low (usually a few meters), which should be flattened now if RMDSs have similar ages with the surrounding mare basalts. Some RMDSs were found in the craters with a low degree of degradation (130–1500 Ma); thus, RMDSs are also potentially very young features [78,79].

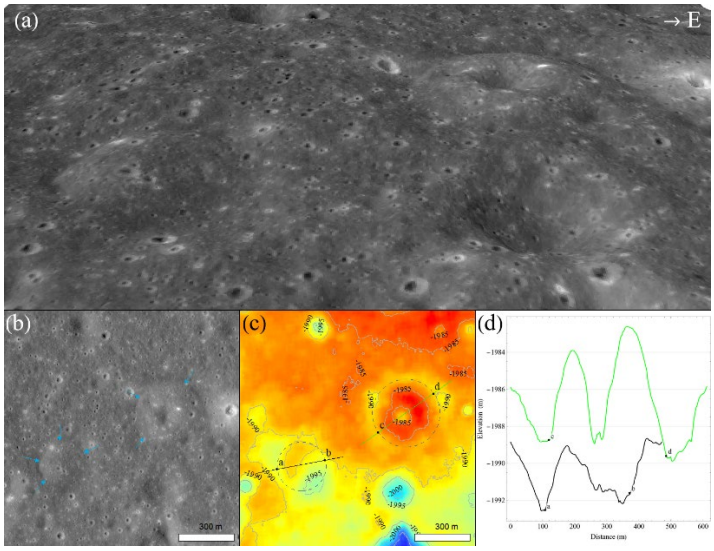

Figure 10. Two RMDSs (1.38°S, 52.27°E and 1.37°S, 52.29°E) in Mare Fecunditatis. (**a**) 3D image of these two RMDSs (five times vertical exaggeration); (**b**) NAC orthoimage; (**c**) NAC DTM; (**d**) elevation of the profiles of (**c**). Data source: NAC M1126787189LE and NAC M106533362LE.

3.2. Tectonic Features

3.2.1. Wrinkle Ridges

A wrinkle ridge is a linear positive relief landform on the lunar surface, which extends up to hundreds of kilometers, mainly distributed in the lunar maria. There are three

main hypotheses on the formation of wrinkle ridges: (1) tectonic origins [80–82]; (2) magmatic origins [83–85]; and (3) tectonic and magmatic origins [85–88]. There are more than two hundred wrinkled ridges (Figure 3) in Mare Fecunditatis [89]. Their lengths vary from 1 km to 250 km; most of them are less than 50 km long, mainly with an NS trend, consistent with the global trend [34].

3.2.2. Arcuate Rilles and Grabens

In addition to the sinuous rilles and floor fractures, the tectonic movement also forms long and narrow grooves, including arcuate rilles and grabens (straight rilles) (Figure 6). Arcuate rilles are usually on the edge of the lunar mare with smooth curves [90]. The graben (straight rilles) forms under the extensional stresses, and a block of the crust cracks and drops down to create the valley floor [91–93].

3.3. Impact Craters

Impact craters are the most common geomorphologic features on the lunar surface. According to their size and shape, craters are divided into simple craters (<20 km, bowl-shaped, Figure 11a), complex craters (tens to hundreds of kilometers, with terraced walls, central peaks, and flat floor), and multi-ringed basins (>290 km, with multiple peak rings) [94]. Impact craters in Mare Fecunditatis are mainly simple impact craters, with several complex impact craters on the edges. There are also some atypical craters such as elliptical craters (Figure 11b), buried craters (Figure 11c), and crater chains (Figure 11d) in Mare Fecunditatis.

Messier Crater (1.9°S, 47.67°E) is an elliptical crater with a major axis ~14.3 km and a minor axis of ~8.3 km, while the Messier A crater (1.97°S, 46.95°E) has a major axis ~15.8 km and a minor axis ~11 km (Figure 11b) [95]. Messier was likely formed by a low-angle westward impact, and Messier A formed following a rebound by the impacting body [96]. Major vertical rays extend over 100 km north and south from Messier and horizontal rays extend over 100 km west from Messier A. The results of Monte Carlo simulations [97] show that the simulating ray patterns by oblique impact are very similar to reality. In addition, there are at least 29 buried impact craters in the Mare Fecunditatis. The crater chains refer to a row of craters distributed linearly. Crater chains formed by secondary craters and collapse of the lava tube are identified in Mare Fecunditatis.

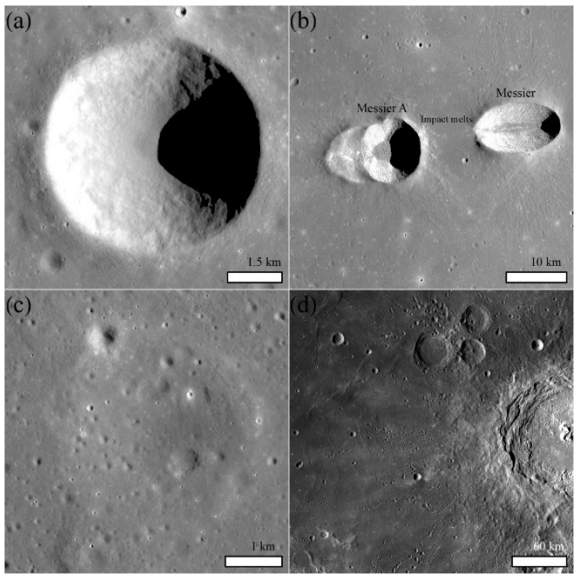

Figure 11. Different types of craters in Mare Fecunditatis. (**a**) A simple crater (0.2°S, 45.5°E), shown with a TC image; (**b**) Messier (1.9°S, 47.7°E), Messier A (1.97°S, 46.95°E), and smooth impact melts, shown with a TC image; (**c**) a buried crater (3.10°N, 53.78°E), shown with a TC image; (**d**) crater chains on the south of Langrenus (8.8°S, 61.2°E), shown with a WAC image.

3.4. Other Features

3.4.1. Pit Craters

Lunar pit craters formed by the collapse of underground space. A total of 15 pit craters have been discovered on the maria and 5 on the highlands [14,98–100]. The underground space may be formed by the lava tube or the stoping of magma [14,100]. Recently, the underground space of the caves in Marius Hills has been detected through radar and gravity analyses [101,102]. Pit craters stay stable for at least tens of years. Some pits (such as King Crater Bridge) found at the Apollo period still show no change with the NAC data [14]. There is a pit crater (0.917°S, 48.660°E, Figure 12) in the center of Fecunditatis, and a highland-type pit crater (6.752°S, 42.759°E, Figure 13) at the southwest.

This paper employs Integrated Software for Imagers and Spectrometers (ISIS) to make the high-resolution NAC DTM (Figures 12c and 13c) of two pit craters. The entrance to the central Mare Fecunditatis pit crater (Figure 12) is about 125 × 100 m in size and 35 m in depth. Deposits lie on the southeast and northwest wall. The deposits on the northwest wall extend ~30 m laterally, with a slope of 20–65°. The southeast wall has collapsed severely, with a relatively gentle slope (10–35°). Most of the deposits are finer than the resolution of the NAC image (~1.1 m), with only a few meter-level rocks at the bottom of the pit crater. The bottom of the pit is relatively flat (<10°), with an area of 27 × 23 m² lower than 15°. The highland pit crater on the southwest side of Mare Fecunditatis (Figure 13) is about 70 m in diameter, and the walls are very steep in all directions. The gentlest southwest wall is 30–60°, and the maximum slope of the northeast wall exceeds 80°. The bottom of the pit is relatively flat (<10°) with an area of 23×10 m².

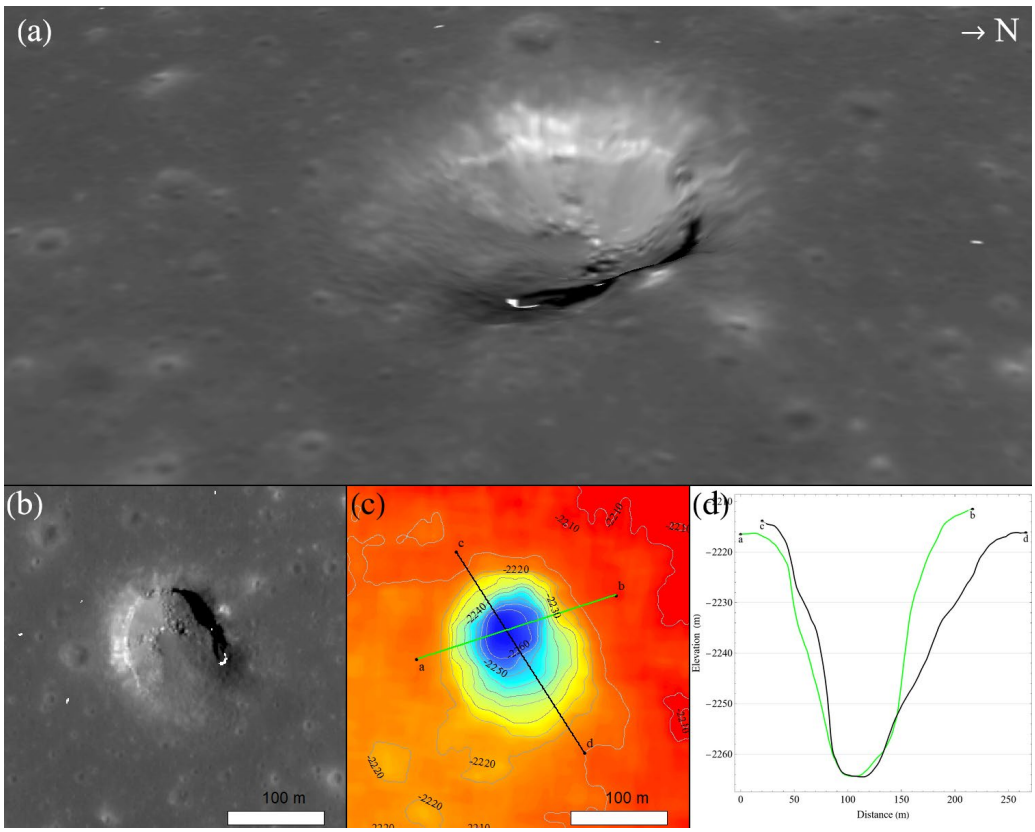

Figure 12. Pit crater (0.917°S, 48.660°E) in the central Fecunditatis. (**a**) 3D image (real elevation values are used); (**b**) NAC orthoimage; (**c**) NAC DTM; (**d**) elevation of the profiles of (**c**). Data source: NAC M1105602888RE and NAC M1197457075RE.

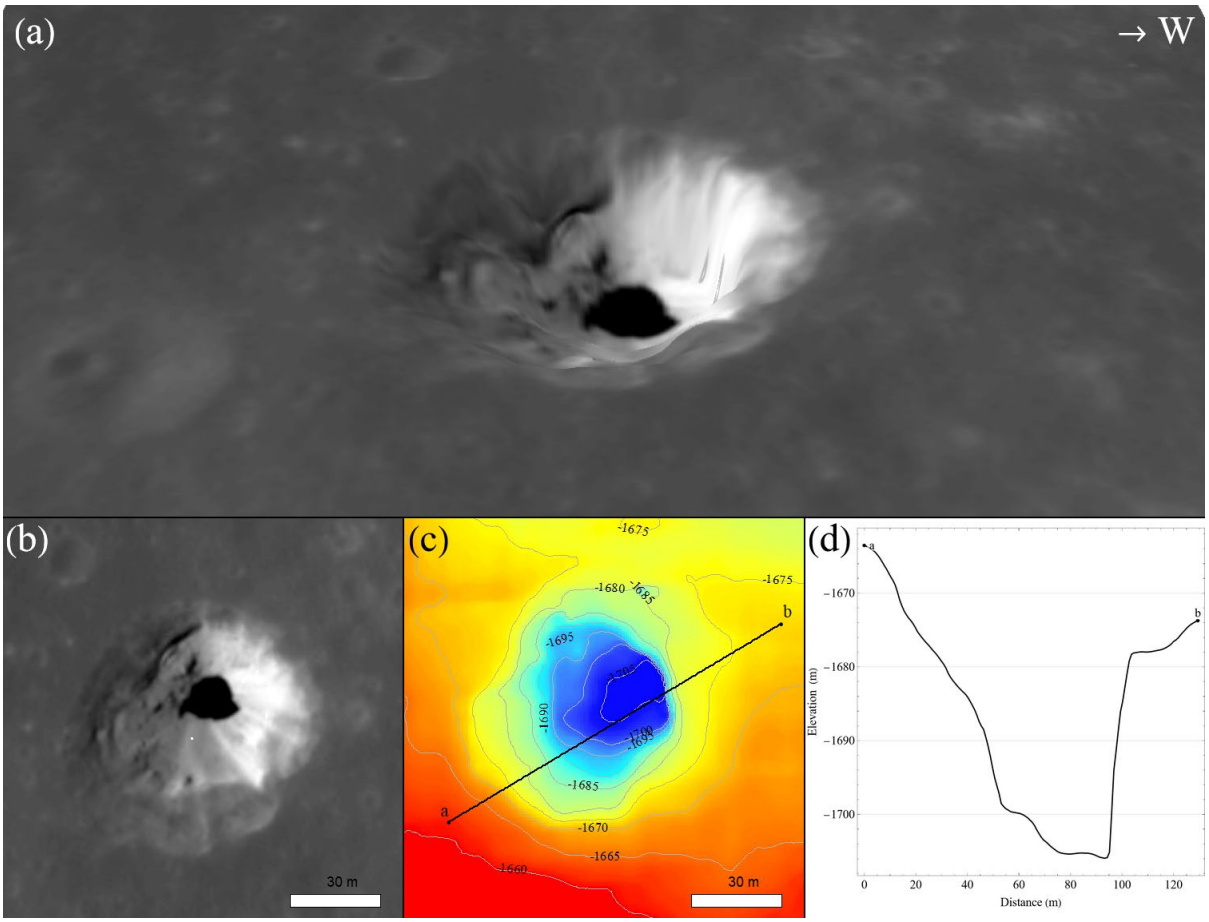

Figure 13. Pit crater (6.752°S, 42.759°E) on the west of Fecunditatis. (**a**) 3D image (real elevation values are used); (**b**) NAC orthoimage; (**c**) NAC DTM; (**d**) elevation of the profiles of (**c**). Data source: NAC M1100931431LE and NAC M1120953701RE.

3.4.2. Swirls

Lunar swirls are high-albedo loops and ribbons occurring in both maria and highlands associated with strong crustal magnetic fields. The formation of the swirls may be related to (1) the magnetic anomalies blocking the solar wind ion bombardment, which reduces the degree of space weathering (darkening with time) [103–106]; (2) comet impacts or micrometeoroid swarms scouring the top-most surface regolith, which exposes fresh material and imparts a remnant magnetization [107–109]; (3) weak electric fields attract the high-albedo, fine-grained, feldspar-rich dust [110]. The interaction between the solar wind and silicate regolith produces water (e.g., [111,112]). Moon Mineralogy Mapper (M^3, [113]) spectral data show that the regolith on the swirl has lower water than the surrounding area [106], which supports the hypothesis (1).

There are three swirls (Figure 14, identified by [19]) on the highland at the southwest side of Mare Fecunditatis with a low optical maturity (OMAT, Figure 14b, [40]), and the surface vector mapping (SVM, [114]) of magnetic field (B-flied) shows this area has a magnitude of up to 100 nT (Figure 14d). The MI mineral data (Figure 14c, [40]) of the swirl show consistent plagioclase with the surrounding area, which contradicts hypothesis (3).

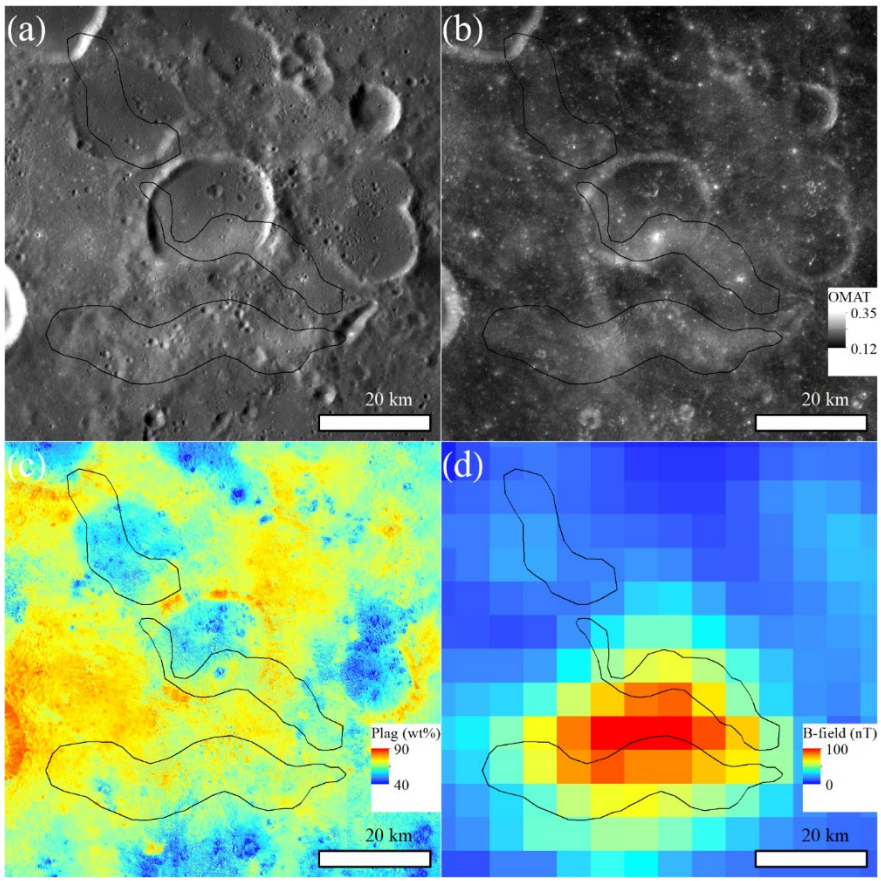

Figure 14. Swirls (14.9°S, 51.8°E) on the west of Mare Fecunditatis. (**a**) WAC image; (**b**) MI OMAT image (brighter tones indicate lower maturity); (**c**) MI Plagioclase abundance; (**d**) SVM magnetic field magnitude map.

4. Discussion

After analyzing the geological features in Mare Fecunditatis, eight targets are selected with high scientific values. First, we summarize their scientific significance and then design a traverse to detect all of these targets for a composite long-distance mission.

4.1. High-Value Detection Targets

4.1.1. Pit Craters

Pit craters are the natural cross-section to the subsurface of mare basalts, which could be used to study multiple eruptions of lunar volcanism and ancient regolith. Pit craters also connect to underground space, which has excellent conditions for the construction of a long-term lunar research station [115,116], such as (1) relatively constant temperature [117,118], (2) low cosmic ray flux [119,120], (3) little lunar dust [98], and (4) shielding from micrometeorite impact [120]. However, the entrance of the pit crater is usually very steep. The pit crater in the middle of Mare Fecunditatis has a collapsed wall (10–35°) comprised of deposits on the southeastern side, which makes it easy to enter the underground space technically. A robot with inflatable composite structures [121] with laser scanners [122] and other payloads may be considered to enter the cave. If successful, this project be the first to enter the moon and investigate in-situ lava outcrops.

4.1.2. Young Volcanism

Crater size–frequency distribution (CSFD) measurements are widely used to date the planetary surface. The CSFD measurements rely heavily on the lunar crater chronology function (e.g., [123–127]), which is based on the returned lunar samples with known

sources. However, due to the lack of young samples (<3 Ga) at the age range of 1–3 Ga, the chronology function maybe not be constrained well [128]. The lunar chronology function is gentle, between 1 and 3 Ga, plus there is a small crater population in the young region, which will bring additional errors of dating a young lunar surface [129]. Although Chang'E-5 brought back some young lunar basalts, with the youngest dating age being ~2.0 Ga [130,131], more samples are needed to better constrain the lunar chronology function within the age between 1.0 and 3.0 Ga. Basalts in Mare Fecunditatis with ages between ~2.2 and ~2.9 Ga are ideal places to constrain the chronology function.

The timing of the latest lunar volcanic activity is extremely important for understanding the thermal evolution history of the Moon. The Moon is expected to cool rapidly and freeze the molten mantle layer quickly after its formation due to its small size [132]. Some authors simulated that the heat is enough to maintain partial melting from the mantle and eruption of mare basalts, until 2.2–3.4 Ga [133]. The youngest mare basalts are mainly distributed in Oceanus Procellarum (e.g., [21,25,134]) with the concentration of heat-producing elements (e.g., [135–137]). However, the 2.0 Ga Chang'E-5 basalts are neither admixing KREEP (enriched in potassium, rare-earth elements, and phosphorus) [130,138,139] nor enriching volatiles [140], raising the question of what derives the late-stage basalts. The young mare basalts within Mare Fecunditatis are far away from the Lunar Procellarum KREEP Terrane (PKT) and may have a distinct origin with Chang'E-5 samples. All of the IMPs are emplaced in the Eratosthenian basalts, and RMDSs are distributed in the Imbrian basalts with TiO_2 > 3 wt% in Mare Fecunditatis; their spatial and time relationship may provide additional clues of the young lunar volcanism. Plenty of in-situ chemical detections, sample returns, and rock dating are required, and it is noteworthy that there may be some sub-meter rocks in IMPs.

4.1.3. High-Al Basalts

Lunar basalt samples have significantly enhanced our understanding of the lunar mantle composition and structures. High-Al basalts are widely distributed across the Moon [45,46]. However, high-Al basalt samples are relatively few (Apollo 12, Luna 16, and one sample each from Apollo 14 and Apollo 16). Moreover, the age of these samples is bimodal, with few 3.4–4.0 Ga-old samples and no 3.5–3.8 Ga-old samples. Remote sensing data show that the southern Mare Fecunditatis is filled with low-Ti (<2 wt%) high-Al basalts of 3.6–3.7 Ga [60], which is distinct from the collected samples. Thus, the high-Al basalts in the southern Mare Fecunditatis could provide samples to study this type of special lunar volcanism.

4.1.4. Pyroclastic Deposits

Pyroclastic deposits result from explosive volcanic eruptions, originating from the deep mantle (~300 to ~400 km) [141,142]. The pyroclastic magma rises faster and may carry some lunar mantle xenoliths. Sample analysis (e.g., [143–146]) and infrared remote sensing data [147,148] showed over a hundred μg/g water in the pyroclastic glasses, indicating the existence of volatile reservoirs in the lunar mantle. More pyroclastic glasses are required to understand the water content and distribution in the lunar mantle. On the other hand, the water in the pyroclastic deposits may be an important in-situ resource.

There are two sites of pyroclastic deposits in the Mare Fecunditatis: (1) one in Crater Taruntius (5.4°N, 46.5°E), whose wall has a relatively high slope (15–30°), but is difficult to access; (2) another in the western region of the Mare Fecunditatis (3.0°S, 42.3°E), which is flat and easy to access.

4.1.5. Swirls

Lunar swirls are essential to understand (1) the history of the lunar core dynamo; (2) the magnetic effects of large-scale impacts; (3) the formation of the swirls; and (4) the specific space weathering effects (including the production of nanophase iron and water) to the regolith with weak solar wind ion bombardment. Hundreds of swirls have been

identified on the lunar mare and highlands. However, none of the swirls have been detected by the in-situ missions. Lunar swirls on the west side of Mare Fecunditatis are across both highland and mare and most areas have a slope less than 15°, which is possible to detect. Swirls near Mare Fecunditatis are across the highlands and maria, which require detailed route planning with high-resolution images (e.g., NAC) and a rover with excellent climbing ability.

4.1.6. Fresh Craters

The nature and extent of lateral and vertical mixing of local and ejecta material are poorly constrained [1]. The eject rays from the fresh craters are less affected by space weathering, and it is easy to separate the young ejecta from local materials if they have distinct compositions. Petavius B (19.9°S, 57.0°E, 32.0 km in diameter), located in the southeastern Mare Fecunditatis, is the ideal target to study the mixing of local and ejected materials. It has a high albedo butterfly-shaped ray pattern stretching ~200 km with low-Fe and low-Ti contents.

In addition, sample returned from impact melts of the fresh crater, such as impact melts (tens of km^2) between Messier and Messier A, would provide additional calibration points at the younger range of the lunar chronology function, as a supplementary of the young impact melt samples of Copernicus, Tycho, North Ray, and Cone craters collected in the Apollo missions.

4.2. Traverse Design for Long-Distance Detection

Here, we envision a long-range exploration mission, referring to previous rovers and the Intrepid [8,149] (Table 1). The concept mission temporarily named Fengfu is under the brainstorming stage, and some content may be unrealistic right now. Most of the high-value detection targets selected in this study are distributed in the center and southern Mare Fecunditatis. A 1408 km traverse (Figure 15; Table 2) is designed with reference to the 60 m spatial resolution SLDEM2015 slope map and 10 m-spatial-resolution TC images [150]. The detection traverse starts from an RMDS (S1-1, 1.31°S, 52.50°E), passing through several RMDSs (S1), domes (S1-4 and S3), pit crater (S2), Messier Crater and its impact melt and ray system (S4), young mare basalt (S5), IMPs (S5), pyroclastic deposits (S6), sinuous rilles (S6), high-Al basalt, swirls (S7), and impact blanket of the Petavius B. The average slope of the traverse is 2.58°, the slope of more than 94% in the traverse is less than 5°, and almost 100% has a slope of less than 10°. After entering the swirl on the highland, the slope is steeper, but still <20°.

Table 1. Travel distance, time, and speed of previous lunar rovers, the Intrepid, and the Fengfu

Rover	Landing Time	Travel Distance	Travel Time	Average Speed	Top Speed
Lunokhod 1	1970	10.54 km	321 days	0.97 km/lunar day	0.1 km/h
Lunar Roving Vehicle (Apollo 15)	1971	27.76 km	3 h 02 min	9.15 km/h	13 km/h
Lunar Roving Vehicle (Apollo 16)	1972	26.55 km	3 h 26 min	7.73 km/h	13 km/h
Lunar Roving Vehicle (Apollo 17)	1972	35.89 km	4 h 26 min	8.10 km/h	13 km/h
Lunokhod 2	1973	39 km	136 days	8.46 km/lunar day	2 km/h
Yutu	2013	0.1148 km	42 days	80.63 m/lunar day	0.2 km/h
Yutu-2	2018	1.0039 km (10 January 2022)	1103 days	26.85 m/lunar day	0.2 km/h
Intrepid	-	1800 km	4 years	37.5 km/lunar day	1 km/h
Fengfu (this study)	-	1400 km	5 years	22.58 km/lunar day	1 km/h

The traverse needs an unmanned rover with scientific payloads and some small robots for sample collections. A small rover is greatly affected by the ambient temperature; for example, Yutu-2 (135 kg) has to finish working at noon due to the high temperature.

Although a large rover is likely to have a good temperature-control system, we assume that the Fengfu rover only has a third of the time (236 h) to work per lunar day and has two working modes: (1) target-exploration mode, focusing on exploring targets and hardly moving; and (2) navigation mode, traveling and detecting passing regolith and rocks. Fifteen lunar days are allotted to the target–exploration mode (Table 2), including five lunar days for the pit crater, and one lunar day for another target. Complex targets (such as pit craters) would be explored in conjunction with astronauts or dedicated robots at the same time—the samples would be returned, and the rover would be repaired. Although the Fengfu could be designed to move very quickly, the rapid movement of the lunar rover faces the risk of dust accumulation [151,152]. If the average navigation speed of the Fengfu is 0.5 km/h (the same as the Intrepid), and (semi-automatically) travels 30 km (60 h) every lunar day, there are another 176 h to explore passing regolith and rocks (roughly traveling for 1 h and exploring for 3 h). It will take ~47 lunar days to finish the navigation. At the end of this mission, the rest of samples would be packeted and returned by another mission. A total of 62 lunar days (~5 years) are required to complete the mission.

Compared with detection targets in the Intrepid mission [8,149], both missions contain IMPs (potential very young volcanism), young basalts (modification the crater chronology curve and understanding the lunar thermal history), pyroclastic deposits (understanding the deep mantle), and swirls (understanding lunar core dynamo and space weathering effects). The targets in our work also include the pit crater (to detect underground space), RMDSs (potential very young volcanism), high-Al basalt (filling the gap between Apollo 14 and Luna 16), and large fresh craters with melt sheet (modification of the crater chronology curve) or distinct composition (understanding the mixture of local and ejecta material processes). The exploration of Mare Fecunditatis is significant to fully understand the history of lunar evolution.

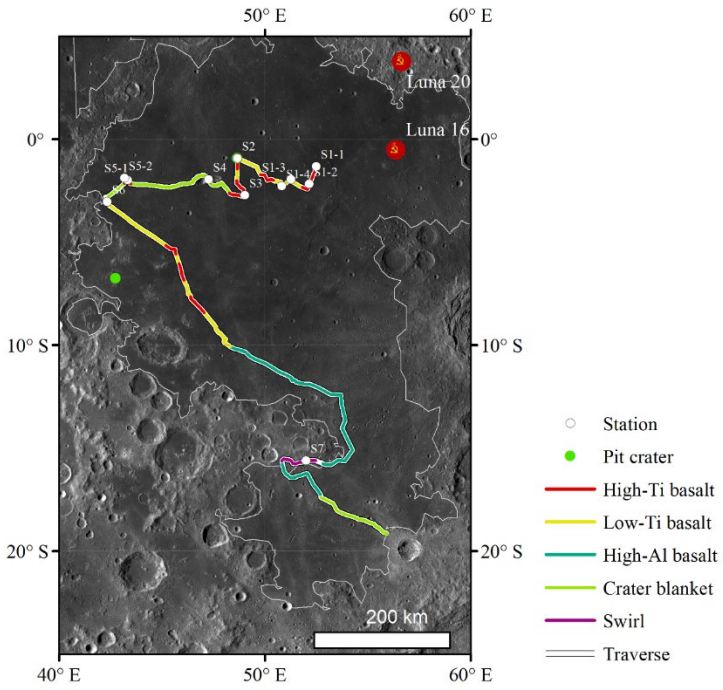

Figure 15. Long-distance detection traverse in Mare Fecunditatis, shown with a WAC image. White points represent the stations in the mission, green points represent the pit craters, and lines with different colors represent segments of the traverse. Considering the error of remote sensing data, in this figure, the high-Ti basalt-traverses are defined as $TiO_2 > 5$ wt% on the WAC TiO_2 map, and high-Al basalt-traverses are defined as $Al_2O_3 > 13$ wt% on the IIM chemical map.

Table 2. Stations of the long-distance detection traverse in Mare Fecunditatis

Station	Latitude	Longitude	Exploration time (Lunar Day)	Description
S1-1	1.31471°S	52.5026°E	1	RMDS (High-Ti)
S1-2	2.16267°S	52.1579°E	1	RMDS (Low-Ti)
S1-3	1.95172°S	51.265°E	1	RMDS (Low-Ti)
S1-4	2.26975°S	50.8258°E	1	RMDS and Dome
S2	0.917°S	48.66°E	5	Pit crater
S3	2.71559°S	49.0189°E	1	Dome
S4	1.94542°S	47.2645°E	1	Impact melt
S5-1	1.883°S	43.176°E	1	IMP in a crater
S5-2	2.16852°S	43.4695°E	1	IMP on the mare
S6	3.04264°S	42.348°E	1	Pyroclastic deposits and Sinuous rilles
S7	15.607°S	51.9968°E	1	Swirl
Exploration traverse: High-Ti basalt, Low-Ti basalt, High-Al basalt, Impact blanket, and Swirl				

5. Conclusions

A long-distance lunar traverse could solve more fundamental scientific questions compared with a nominal short-distance mission. Mare Fecunditatis has a multitude of high-value features and a flat terrain, which is very suitable for long-distance detection. In total, several outstanding detection targets are selected: (1) pit crater may connect vast underground void space, which is an ideal place to build a research station; (2) young basalts (2.2–2.9 Ga) and the impact melts of Messier Crater may modify the chronology functions; (3) young basalts and potential very young volcanism (IMP and RMDS) are key to the thermal evolution history of the Moon; (4) basalts in the southern Fecunditatis may be a type of high-Al basalt that differs from previous samples; (5) pyroclastic deposits are windows to understanding the composition of the deep mantle; (6) swirls and magnetic anomalies are important to the history of lunar core dynamo and space weathering effects; and (7)the ray system of the fresh crater may disclose the mixing of local and ejecta material processes. Based on this, a ~1408 km traverse over 5 years has been proposed to explore Mare Fecunditatis, which may help future planning of this class of long-distance missions on the lunar surface.

Author Contributions: Conceptualization, L.X.; methodology, S.Z.; investigation, S.Z.; writing—original draft preparation, S.Z.; writing—review and editing, S.Z., Y.Q., L.X., J.Z., Q.H., J.H., J.W., H.C. and W.X.; visualization, S.Z.; funding acquisition, L.X. All authors have read and agreed to the published version of the manuscript.

Funding: This research was funded by the National Key R & D Program of China (2020YFE0202100) MOST Special Fund from the State Key Laboratory of Geological Processes and Mineral Resources, China University of Geosciences (MSFGPMR05), and the 111 project of China (BP0820004).

Data Availability Statement: The WAC images, NAC images, SLDEM2015, Clementine color ratio map, WAC TiO_2 map, and MI mineral and composition maps are available at PDS Geosciences Node (https://pds-geosciences.wustl.edu/). The TC images and TCDTM are available at SELENE Data Archive (https://darts.isas.jaxa.jp/planet/pdap/selene/index.html.en). The IIM chemical maps are available at https://mega.nz/#F!6ThgVK6a!_x1Pq1p5UW4SVvbK640wow. The SVM magnetic field maps are available at http://www.geo.titech.ac.jp/lab/tsunakawa/Kaguya_LMAG.

Acknowledgments: The authors would like to thank three anonymous reviewers for their insightful and constructive comments and suggestions.

Conflicts of Interest: The authors declare no conflict of interest.

References

1. National Research Council. *The Scientific Context for Exploration of the Moon*; The National Academies Press: Washington, DC, 2007, ISBN 978-0-309-10919-2.
2. Flahaut, J.; Blanchette-Guertin, J.-F.; Jilly, C.; Sharma, P.; Souchon, A.; van Westrenen, W.; Kring, D.A. Identification and characterization of science-rich landing sites for lunar lander missions using integrated remote sensing observations. *Adv. Space Res.* **2012**, *50*, 1647–1665. https://doi.org/10.1016/j.asr.2012.05.020.
3. Jawin, E.R.; Valencia, S.N.; Watkins, R.N.; Crowell, J.M.; Neal, C.R.; Schmidt, G. Lunar Science for Landed Missions Workshop Findings Report. *Earth Space Sci.* **2019**, *6*, 2–40. https://doi.org/10.1029/2018EA000490.
4. Kring, D.A.; Durda, D.D. (Eds.) *A Global Lunar Landing Site Study to Provide the Scientific Context for Exploration of the Moon;* National Academies Press: Washington, DC, USA, 2012.
5. Hiesinger, H.; van der Bogert, C.H.; Wedler, A.; Jaumann, R.; Mall, U.; Head, J.W.; Anand, M.; Jolliff, B.; Pinet, P.; Xiao, L.; et al. The Rima Bode Region—Candidate for a Future Lunar Landing Site. In Proceedings of the 52nd Lunar and Planetary Science Conference, Virtual Event, 15–19 March 2021; p. 1485.
6. Flahaut, J.; Carpenter, J.; Williams, J.-P.; Anand, M.; Crawford, I.A.; van Westrenen, W.; Füri, E.; Xiao, L.; Zhao, S. Regions of interest (ROI) for future exploration missions to the lunar South Pole. *Planet. Space Sci.* **2019**, *180*, 104750. https://doi.org/10.1016/j.pss.2019.104750.
7. Lemelin, M.; Blair, D.M.; Roberts, C.E.; Runyon, K.D.; Nowka, D.; Kring, D.A. High-priority lunar landing sites for in situ and sample return studies of polar volatiles. *Planet. Space Sci.* **2014**, *101*, 149–161. https://doi.org/10.1016/j.pss.2014.07.002.
8. Robinson, M.S.; Blewett, D.T.; Frank, E.; Illsley, P.; Lawrence, S.; Mahanti, P.; Rampe, E.B.; Speyerer, E.J.; Stopar, J.; Tikoo, S.; et al. Intrepid: Lunar Roving Prospector. In Proceedings of the AGU Fall Meeting, San Francisco, CA, USA, 9–13 December 2019; American Geophysical Union: Washington, DC, USA, 2019; p. P33D-03.
9. Zhang, C.; Xu, W.; Wang, Y. Development Ideas of Manned Lunar Surface Exploration. *Aerosp. Shanghai* **2021**, *38*, 109–118. https://doi.org/10.19328/j.cnki.2096-8655.2021.03.013.
10. Wilhelms, D.E.; McCauley, J.F. *Geologic Map of the Near Side of the MOON*; IMAP 1971; USGS: Reston, VI, USA https://doi.org/10.3133/i703.
11. Wilhelms, D.E.; McCauley, J.F.; Trask, N.J. *The Geologic History of the Moon*; Professional Paper, 1987; USGS: Reston, VI, USA. https://doi.org/10.3133/pp1348.
12. Hiesinger, H.; Head, J.W.; Wolf, U.; Jaumann, R.; Neukum, G. New Ages for Basalts in Mare Fecunditatis Based on Crater Size-Frequency Measurements. In Proceedings of the 37th Lunar and Planetary Science Conference, The Woodlands, Houston, Texas, 13–27 March 2006; p. 1151.
13. Robinson, M.S.; Brylow, S.M.; Tschimmel, M.; Humm, D.; Lawrence, S.J.; Thomas, P.C.; Denevi, B.W.; Bowman-Cisneros, E.; Zerr, J.; Ravine, M.A.; et al. Lunar Reconnaissance Orbiter Camera (LROC) Instrument Overview. *Space Sci. Rev.* **2010**, *150*, 81–124. https://doi.org/10.1007/s11214-010-9634-2.
14. Wagner, R.V.; Robinson, M.S. Occurrence and Origin of Lunar Pits: Observations from a New Catalog. In Proceedings of the 52nd Lunar and Planetary Science Conference, Virtual Event, 15–19 March 2021.
15. Braden, S.E.; Stopar, J.D.; Robinson, M.S.; Lawrence, S.J.; van der Bogert, C.H.; Hiesinger, H. Evidence for basaltic volcanism on the Moon within the past 100 million years. *Nat. Geosci.* **2014**, *7*, 787–791. https://doi.org/10.1038/ngeo2252.
16. Zhang, F.; Head, J.W.; Wöhler, C.; Bugiolacchi, R.; Wilson, L.; Basilevsky, A.T.; Grumpe, A.; Zou, Y.L. Ring-Moat Dome Structures (RMDSs) in the Lunar Maria: Statistical, Compositional, and Morphological Characterization and Assessment of Theories of Origin. *J. Geophys. Res.* **2020**, *125*, e2019JE005967. https://doi.org/10.1029/2019JE005967.
17. Gaddis, L.R.; Staid, M.I.; Tyburczy, J.A.; Hawke, B.; Petro, N.E. Compositional analyses of lunar pyroclastic deposits. *Icarus* **2003**, *161*, 262–280. https://doi.org/10.1016/S0019-1035(02)00036-2.
18. Gustafson, J.O.; Bell, J.F.; Gaddis, L.R.; Hawke, B.R.; Giguere, T.A. Characterization of previously unidentified lunar pyroclastic deposits using Lunar Reconnaissance Orbiter Camera data. *J. Geophys. Res.* **2012**, *117*, e12. https://doi.org/10.1029/2011JE003893.
19. Denevi, B.W.; Robinson, M.S.; Boyd, A.K.; Blewett, D.T.; Klima, R.L. The distribution and extent of lunar swirls. *Icarus* **2016**, *273*, 53–67. https://doi.org/10.1016/j.icarus.2016.01.017.
20. Ravi, S.; Meyer, H.M.; Mahanti, P.; Robinson, M.S. On the usefulness of optical maturity for relative age classification of fresh craters. In Proceedings of the AGU Fall Meeting, San Francisco, CA, USA, 12–16 December 2016; p. P53A-2166.
21. Hiesinger, H.; Head, J.W.; Wolf, U.; Jaumann, R.; Neukum, G. Ages and stratigraphy of lunar mare basalts: A synthesis. In *Geological Society of America Special Papers: Recent Advances and Current Research Issues in Lunar Stratigraphy*; Geological Society of America: Boulder, CO, USA, 2011; p. 477. https://doi.org/10.1130/2011.2477(01).
22. Hiesinger, H.; Head, J.W. Ages and stratigraphy of mare basalts in Oceanus Procellarum, Mare Nubium, Mare Cognitum, and Mare Insularum. *J. Geophys. Res.* **2003**, *108*, e7. https://doi.org/10.1029/2002JE001985.
23. Hiesinger, H.; Head, J.W.; Wolf, U.; Jaumann, R.; Neukum, G. Lunar mare basalt flow units: Thicknesses determined from crater size-frequency distributions. *Geophys. Res. Lett.* **2002**, *29*, 89-1–89-4. https://doi.org/10.1029/2002GL014847.
24. Hiesinger, H.; Head, J.W.; Wolf, U.; Jaumann, R.; Neukum, G. Ages and stratigraphy of lunar mare basalts in Mare Frigoris and other nearside maria based on crater size-frequency distribution measurements. *J. Geophys. Res.* **2010**, *115*, e3. https://doi.org/10.1029/2009JE003380.
25. Hiesinger, H.; Jaumann, R.; Neukum, G.; Head, J.W. Ages of mare basalts on the lunar nearside. *J. Geophys. Res.* **2000**, *105*, 29239–29275. https://doi.org/10.1029/2000JE001244.

26. Barker, M.K.; Mazarico, E.; Neumann, G.A.; Zuber, M.T.; Haruyama, J.; Smith, D.E. A new lunar digital elevation model from the Lunar Orbiter Laser Altimeter and SELENE Terrain Camera. *Icarus* **2016**, *273*, 346–355. https://doi.org/10.1016/j.icarus.2015.07.039.
27. McCauley, J.F.; Scott, D.H. The geologic setting of the Luna 16 landing site. *Earth Planet. Sci. Lett.* **1972**, *13*, 225–232. https://doi.org/10.1016/0012-821X(72)90099-4.
28. Rosenburg, M.A.; Aharonson, O.; Head, J.W.; Kreslavsky, M.A.; Mazarico, E.; Neumann, G.A.; Smith, D.E.; Torrence, M.H.; Zuber, M.T. Global surface slopes and roughness of the Moon from the Lunar Orbiter Laser Altimeter. *J. Geophys. Res.* **2011**, *116*, E11007. https://doi.org/10.1029/2010JE003716.
29. Zuber, M.T.; Smith, D.E.; Zellar, R.S.; Neumann, G.A.; Sun, X.; Katz, R.B.; Kleyner, I.; Matuszeski, A.; McGarry, J.F.; Ott, M.N.; et al. The Lunar Reconnaissance Orbiter Laser Ranging Investigation. *Space Sci. Rev.* **2010**, *150*, 63–80. https://doi.org/10.1007/s11214-009-9511-z.
30. Smith, D.E.; Zuber, M.T.; Jackson, G.B.; Cavanaugh, J.F.; Neumann, G.A.; Riris, H.; Sun, X.; Zellar, R.S.; Coltharp, C.; Connelly, J.; et al. The Lunar Orbiter Laser Altimeter Investigation on the Lunar Reconnaissance Orbiter Mission. *Space Sci. Rev.* **2010**, *150*, 209–241. https://doi.org/10.1007/s11214-009-9512-y.
31. Muller, P.M.; Sjogren, W.L. Mascons: Lunar Mass Concentrations. *Science* **1968**, *161*, 680–684. https://doi.org/10.1126/science.161.3842.680.
32. Neumann, G.A.; Zuber, M.T.; Wieczorek, M.A.; Head, J.W.; Baker, D.M.H.; Solomon, S.C.; Smith, D.E.; Lemoine, F.G.; Mazarico, E.; Sabaka, T.J.; et al. Lunar impact basins revealed by Gravity Recovery and Interior Laboratory measurements. *Sci. Adv.* **2015**, *1*, e1500852. https://doi.org/10.1126/sciadv.1500852.
33. Hurwitz, D.M.; Head, J.W.; Hiesinger, H. Lunar sinuous rilles: Distribution, characteristics, and implications for their origin. *Planet. Space Sci.* **2013**, *79–80*, 1–38. https://doi.org/10.1016/j.pss.2012.10.019.
34. Yue, Z.; Li, W.; Di, K.; Liu, Z.; Liu, J. Global mapping and analysis of lunar wrinkle ridges. *J. Geophys. Res.* **2015**, *120*, 978–994. https://doi.org/10.1002/2014JE004777.
35. Jozwiak, L.M.; Head, J.W.; Zuber, M.T.; Smith, D.E.; Neumann, G.A. Lunar floor-fractured craters: Classification, distribution, origin and implications for magmatism and shallow crustal structure. *J. Geophys. Res.* **2012**, *117*, 6. https://doi.org/10.1029/2012JE004134.
36. Rajmon, D.; Spudis, P. Distribution and stratigraphy of basaltic units in Maria Tranquillitatis and Fecunditatis: A Clementine perspective. *Meteorit. Planet. Sci.* **2004**, *39*, 1699–1720. https://doi.org/10.1111/j.1945-5100.2004.tb00067.x.
37. Dehon, R.A. Mare Fecunditatis: Basin Configuration. In Proceedings of the Conference on Origins of Mare Basalts and Their Implications for Lunar Evolution, The Woodlands, Houston, TX, USA, 17–19 November 1975; Lunar Science Institute: Houston, TX, USA, 1975; p. 32.
38. Ohtake, M.; Haruyama, J.; Matsunaga, T.; Yokota, Y.; Morota, T.; Honda, C. Performance and scientific objectives of the SELENE (KAGUYA) Multiband Imager. *Earth Planets Space* **2008**, *60*, 257–264. https://doi.org/10.1186/BF03352789.
39. Otake, H.; Ohtake, M.; Hirata, N. Lunar Iron and Titanium Abundance Algorithms Based on SELENE (Kaguya) Multiband Imager Data. In Proceedings of the 43rd Lunar and Planetary Science Conference, The Woodlands, Houston, TX, USA, 19–23 March 2012; p. 1905.
40. Lemelin, M.; Lucey, P.G.; Gaddis, L.R.; Hare, T.; Ohtake, M. Global Map Products from the Kaguya Multiband Imager at 512 ppd: Minerals, FeO, and OMAT. In Proceedings of the 47th Lunar and Planetary Science Conference, The Woodlands, Houston, TX, USA, 21–25 March 2016; p. 2994.
41. Sato, H.; Robinson, M.S.; Lawrence, S.J.; Denevi, B.W.; Hapke, B.; Jolliff, B.L.; Hiesinger, H. Lunar mare TiO2 abundances estimated from UV/Vis reflectance. *Icarus* **2017**, *296*, 216–238. https://doi.org/10.1016/j.icarus.2017.06.013.
42. Wu, Y.; Besse, S.; Li, J.-Y.; Combe, J.-P.; Wang, Z.; Zhou, X.; Wang, C. Photometric correction and in-flight calibration of Chang' E-1 Interference Imaging Spectrometer (IIM) data. *Icarus* **2013**, *222*, 283–295. https://doi.org/10.1016/j.icarus.2012.11.010.
43. Ouyang, Z.; Li, C.; Zou, Y.; Zhang, H.; Lü, C.; Liu, J.; Liu, J.; Zuo, W.; Su, Y.; Wen, W.; et al. Primary scientific results of Chang'E-1 lunar mission. *Sci. China Earth Sci.* **2010**, *53*, 1565–1581. https://doi.org/10.1007/s11430-010-4056-2.
44. Xia, W.; Wang, X.; Zhao, S.; Jin, H.; Chen, X.; Yang, M.; Wu, X.; Hu, C.; Zhang, Y.; Shi, Y.; et al. New maps of lunar surface chemistry. *Icarus* **2019**, *321*, 200–215. https://doi.org/10.1016/j.icarus.2018.10.031.
45. Kramer, G.Y.; Jolliff, B.L.; Neal, C.R. Distinguishing high-alumina mare basalts using Clementine UVVIS and Lunar Prospector GRS data: Mare Moscoviense and Mare Nectaris. *J. Geophys. Res.* **2008**, *113*, 10. https://doi.org/10.1029/2006JE002860.
46. Kramer, G.Y.; Jolliff, B.L.; Neal, C.R. Searching for high alumina mare basalts using Clementine UVVIS and Lunar Prospector GRS data: Mare Fecunditatis and Mare Imbrium. *Icarus* **2008**, *198*, 7–18. https://doi.org/10.1016/j.icarus.2008.06.009.
47. Kurat, G.; Kracher, A.; Keil, K.; Warner, R.; Prinz, M. Composition and origin of Luna 16 aluminous mare basalts. In *Lunar and Planetary Science Conference Proceedings*; Pergamon Press: New York, NY, USA, 1976; Volume 2, pp. 1301–1321.
48. Ma, M.-S.; Schmitt, R.A.; Nielsen, R.L.; Taylor, G.J.; Warner, R.D.; Keil, K. Petrogenesis of Luna 16 aluminous Mare basalts. *Geophys. Res. Lett.* **1979**, *6*, 909–912. https://doi.org/10.1029/GL006i011p00909.
49. Huneke, J.C.; Podosek, F.A.; Wasserburg, G.J. Gas retention and cosmic-ray exposure ages of a basalt fragment from Mare Fecunditatis. *Earth Planet. Sci. Lett.* **1972**, *13*, 375–383. https://doi.org/10.1016/0012-821X(72)90112-4.
50. Cadogan, P.H.; Turner, G. 40Ar-39Ar dating of Luna 16 and Luna 20 samples. *Phil. Trans. R. Soc. Lond. A* **1977**, *284*, 167–177. https://doi.org/10.1098/rsta.1977.0007.

51. Cohen, B.A.; Snyder, G.A.; Hall, C.M.; Taylor, L.A.; Nazarov, M.A. Argon-40-argon-39 chronology and petrogenesis along the eastern limb of the Moon from Luna 16, 20 and 24 samples. *Meteorit. Planet. Sci.* **2001**, *36*, 1345–1366. https://doi.org/10.1111/j.1945-5100.2001.tb01829.x.
52. Fernades, V.A.; Burgess, R. Volcanism in Mare Fecunditatis and Mare Crisium: Ar-Ar age studies. *Geochim. Cosmochim. Acta* **2005**, *69*, 4919–4934. https://doi.org/10.1016/j.gca.2005.05.017.
53. Haruyama, J.; Ohtake, M.; Matsunaga, T.; Morota, T.; Yokota, Y.; Honda, C.; Hirata, N.; Demura, H.; Iwasaki, A.; Nakamura, R.; et al. Planned radiometrically calibrated and geometrically corrected products of lunar high-resolution Terrain Camera on SELENE. *Adv. Space Res.* **2008**, *42*, 310–316. https://doi.org/10.1016/j.asr.2007.04.062.
54. Greeley, R. Lunar hadley rille: Considerations of its origin. *Science* **1971**, *172*, 722–725. https://doi.org/10.1126/science.172.3984.722.
55. Jozwiak, L.M.; Head III, J.W.; Neumann, G.A.; Wilson, L. Observational constraints on the identification of shallow lunar magmatism: Insights from floor-fractured craters. *Icarus* **2017**, *283*, 224–231. https://doi.org/10.1016/j.icarus.2016.04.020.
56. Jozwiak, L.M.; Head, J.W.; Wilson, L. Lunar floor-fractured craters as magmatic intrusions: Geometry, modes of emplacement, associated tectonic and volcanic features, and implications for gravity anomalies. *Icarus* **2015**, *248*, 424–447. https://doi.org/10.1016/j.icarus.2014.10.052.
57. Hall, J.L.; Solomon, S.C.; Head, J.W. Lunar floor-fractured craters: Evidence for viscous relaxation of crater topography. *J. Geophys. Res.: Solid Earth* **1981**, *86*, 9537–9552. https://doi.org/10.1029/JB086iB10p09537.
58. Wichman, R.W.; Schultz, P.H. Floor-fractured craters in Mare Smythii and west of Oceanus Procellarum: Implications of crater modification by viscous relaxation and igneous intrusion models. *J. Geophys. Res.* **1995**, *100*, 21201–21218. https://doi.org/10.1029/95JE02297.
59. Dombard, A.J.; Gillis, J.J. Testing the viability of topographic relaxation as a mechanism for the formation of lunar floor-fractured craters. *J. Geophys. Res.* **2001**, *106*, 27901–27909. https://doi.org/10.1029/2000JE001388.
60. Hiesinger, H.; Head, J.W. New Views of Lunar Geoscience: An Introduction and Overview. *Rev. Mineral. Geochem.* **2006**, *60*, 1–81. https://doi.org/10.2138/rmg.2006.60.1.
61. Gaddis, L.R. Progress toward characterization of juvenile materials in lunar pyroclastic deposits. In *Workshop on New Views of the Moon 2: Understanding the Moon Through the Integration of Diverse Datasets*; Gaddis, L., Shearer, C.K., Eds.; Lunar and Planetary Institute: Houston, TX, USA, 1999.
62. Spudis, P.D. Young dark mantle deposits on the Moon. In Proceedings of the Workshop on Lunar Volcanic Glasses: Scientific and Resource Potential, Houston, TX, USA, 10–11 October 1989; LPI Technical Report 90-02; Delano, J.W., Heiken, G.H., Eds.; Lunar and Planetary Institute: Houston, TX, USA, 1990; p. 60.
63. Whitaker, E.A. An Unusual Mare Feature. In *Apollo 15: Preliminary Science Report*; Swann, G.A., Bailey, N.G., Batson, R.M., Freeman, V.L., Hait, M.H., Head, J.W., Holt, H.E., Howard, K.A., Irwin, J.B., Larson, K.B., Muehlberger, W.R., Eds.; NASA: Washington, DC, USA, 1972; p. 84.
64. El-Baz, F. New geological findings in Apollo 15 lunar orbital photography. In Proceedings of the Third Lunar Science Conference, Houston, TX, USA, 10 January 1972.
65. El-Baz, F. "D-Caldera": New Photographs of a Unique Feature. In *Apollo 17: Preliminary Science Report*; Renner, K., Ed.; NASA: Washington, DC, USA, 1973.
66. Strain, P.L.; El-Baz, F. The geology and morphology of Ina. In Proceedings of the 11th Lunar and Planetary Science Conference, The Woodlands, Houston, TX, USA, 17–21 March 1980; Pergamon Press: New York, NY, USA, 1980; pp. 2437–2446.
67. Schultz, P.H.; Staid, M.I.; Pieters, C.M. Lunar activity from recent gas release. *Nature* **2006**, *444*, 184–186. https://doi.org/10.1038/nature05303.
68. Garry, W.B.; Robinson, M.S.; Zimbelman, J.R.; Bleacher, J.E.; Hawke, B.R.; Crumpler, L.S.; Braden, S.E.; Sato, H. The origin of Ina: Evidence for inflated lava flows on the Moon. *J. Geophys. Res.* **2012**, *117*, e12. https://doi.org/10.1029/2011JE003981.
69. Carter, L.M.; Hawke, B.R.; Garry, W.B.; Campbell, B.A.; Giguere, T.A.; Bussey, D.B.J. Radar Observations of Lunar Hollow Terrain. In Proceedings of the 44th Lunar and Planetary Science Conference, The Woodlands, Houston, TX, USA, 18–22 March 2013; p. 2146.
70. Qiao, l.; Head, J.; Wilson, L.; Xiao, L.; Kreslavsky, M.; Dufek, J. Ina pit crater on the Moon: Extrusion of waning-stage lava lake magmatic foam results in extremely young crater retention ages. *Geology* **2017**, *45*, 455–458. https://doi.org/10.1130/G38594.1.
71. Wilson, L.; Head, J.W. Eruption of magmatic foams on the Moon: Formation in the waning stages of dike emplacement events as an explanation of "irregular mare patches". *J. Volcanol. Geotherm. Res.* **2017**, *335*, 113–127. https://doi.org/10.1016/j.jvolgeores.2017.02.009.
72. Qiao, l.; Head, J.W.; Xiao, L.; Wilson, L.; Dufek, J.D. The role of substrate characteristics in producing anomalously young crater retention ages in volcanic deposits on the Moon: Morphology, topography, subresolution roughness, and mode of emplacement of the Sosigenes lunar irregular mare patch. *Meteorit. Planet. Sci.* **2018**, *53*, 778–812. https://doi.org/10.1111/maps.13003.
73. Qiao, l.; Head, J.W.; Ling, Z.; Wilson, L.; Xiao, L.; Dufek, J.D.; Yan, J. Geological Characterization of the Ina Shield Volcano Summit Pit Crater on the Moon: Evidence for Extrusion of Waning-Stage Lava Lake Magmatic Foams and Anomalously Young Crater Retention Ages. *J. Geophys. Res.* **2019**, *124*, 1100–1140. https://doi.org/10.1029/2018JE005841.
74. Head, J.W.; Wilson, L. Generation, ascent and eruption of magma on the Moon: New insights into source depths, magma supply, intrusions and effusive/explosive eruptions (Part 2: Predicted emplacement processes and observations). *Icarus* **2017**, *283*, 176–223. https://doi.org/10.1016/j.icarus.2016.05.031.

75. Wöhler, C.; Lena, R.; Lazzarotti, P.; Phillips, J.; Wirths, M.; Pujic, Z. A combined spectrophotometric and morphometric study of the lunar mare dome fields near Cauchy, Arago, Hortensius, and Milichius. *Icarus* **2006**, *183*, 237–264. https://doi.org/10.1016/j.icarus.2006.03.003.
76. Huang, Q.; Zhao, J.; Wang, X.; Wang, T.; Zhang, F.; Le Qiao; Chen, Y.; Qiu, D.; Yang, Y.; Xiao, L. A large long-lived central-vent volcano in the Gardner region: Implications for the volcanic history of the nearside of the Moon. *Earth Planet. Sci. Lett.* **2020**, *542*, 116301. https://doi.org/10.1016/j.epsl.2020.116301.
77. Zhang, F.; Head, J.W.; Basilevsky, A.T.; Bugiolacchi, R.; Komatsu, G.; Wilson, L.; Fa, W.; Zhu, M.-H. Newly Discovered Ring-Moat Dome Structures in the Lunar Maria: Possible Origins and Implications. *Geophys. Res. Lett.* **2017**, *44*, 9216–9224. https://doi.org/10.1002/2017GL074416.
78. Basilevsky, A.T.; Zhang, F.; Wöhler, C.; Bugiolacchi, R.; Head, J.W.; Wilson, L. Lunar Ring-Moat Dome Structures and Their Relationships with Small Impact Craters. In Proceedings of the 50th Lunar and Planetary Science Conference, The Woodlands, Houston, TX, USA, 2019; p. 1507.
79. Zhang, F.; Head, J.W.; Wöhler, C.; Basilevsky, A.T.; Wilson, L.; Xie, M.; Bugiolacchi, R.; Wilhelm, T.; Althoff, S.; Zou, Y.L. The Lunar Mare Ring-Moat Dome Structure (RMDS) Age Conundrum: Contemporaneous with Imbrian-Aged Host Lava Flows or Emplaced in the Copernican? *J. Geophys. Res. Planets* **2021**, *126*, e2021JE006880. https://doi.org/10.1029/2021JE006880.
80. Bryan, W.B. Wrinkle-ridges as deformed surface crust on ponded mare lava. In Proceedings of the Fourth Lunar Science Conference, The Woodlands, Houston, TX, USA, 17 March 1973; Pergamon Press: New York, NY, USA, 1973.
81. Howard, K.A.; Muehlberger, W.R. Mare ridges and related studies: Part C: Lunar thrust faults in the Taurus-Littrow region. In *Apollo 17: Preliminary Science Report*; Renner, K., Ed.; NASA: Washington, DC, USA, 1973.
82. Lucchitta, B.K. Mare ridges and related highland scarps-Result of vertical tectonism. In Proceedings of the Seventh Lunar Science Conference, Houston, TX, USA, 15–19 March 1976.
83. Quaide, W. Rilles, ridges, and domes—Clues to maria history. *Icarus* **1965**, *4*, 374–389. https://doi.org/10.1016/0019-1035(65)90041-2.
84. Strom, R.G. Lunar Mare Ridges, Rings and Volcanic Ring Complexes. In *The Moon, Proceedings from IAU Symposium no. 47, the University of Newcastle-Upon-Tyne England, 22–26 March 1971*; Runcorn, S.K., Urey, H.C., Eds.; Springer International Publishing: Cham, Switzerland, 1972; pp. 187–215, ISBN 978-94-010-2861-5.
85. Scott, D.H. Mare ridges and related studies: Part D: Small structures of the Taurus-Littrow region. In *Apollo 17: Preliminary Science Report*; Renner, K., Ed.; NASA: Washington, DC, USA, 1973.
86. Young, R.A.; Brennan, W.J.; Wolfe, R.W.; Nichols, D.J. Mare ridges and related studies: Part A: Volcanism in the lunar maria. In *Apollo 17: Preliminary Science Report*; Renner, K., Ed.; NASA: Washington, DC, USA, 1973.
87. Scott, D.H.; Diaz, J.M.; Watkins, J.A. The geologic evaluation and regional synthesis of metric and panoramic photographs. In Proceedings of the Sixth Lunar Science Conference, Houston, TX, USA, 17–21 March 1975; pp. 2531–2540.
88. Yue, Z.; Michael, G.G.; Di, K.; Liu, J. Global survey of lunar wrinkle ridge formation times. *Earth Planet. Sci. Lett.* **2017**, *477*, 14–20. https://doi.org/10.1016/j.epsl.2017.07.048.
89. Thompson, T.J.; Robinson, M.S.; Watters, T.R.; Johnson, M.B. Global Lunar Wrinkle Ridge Identification and Analysis. In Proceedings of the 48th Lunar and Planetary Science Conference, The Woodlands, Houston, TX, USA, 20-24 Mar 2017; p. 2665.
90. Maxwell, T.A.; El-Baz, F.; Ward, S.H. Distribution, Morphology, and Origin of Ridges and Arches in Mare Serenitatis. *Geol. Soc. Am. Bull.* **1975**, *86*, 1273. https://doi.org/10.1130/0016-7606(1975)86<1273:DMAOOR>2.0.CO;2.
91. Fielder, G. Topography and tectonics of the lunar straight wall. *Planet. Space Sci.* **1963**, *11*, 23–30. https://doi.org/10.1016/0032-0633(63)90200-9.
92. Middlehurst, B.M. Lunar Tidal Phenomena and the Lunar Rille System. In *The Moon, Proceedings from IAU Symposium no. 47, the University of Newcastle-Upon-Tyne, UK, 22–26 March 1971*; Runcorn, S.K., Urey, H.C., Eds.; Springer International Publishing: Cham, Switzerland, 1972; pp. 450–457, ISBN 978-94-010-2861-5.
93. Solomon, S.C.; Head, J.W. Vertical movement in mare basins: Relation to mare emplacement, basin tectonics, and lunar thermal history. *J. Geophys. Res.: Solid Earth* **1979**, *84*, 1667–1682. https://doi.org/10.1029/JB084iB04p01667.
94. Melosh, H.J. *Impact Cratering: A Geologic Process*; Oxford University Press: New York, NY, USA, 1989; ISBN 9780195042849.
95. Herrick, R.R.; Forsberg-Taylor, N.K. The shape and appearance of craters formed by oblique impact on the Moon and Venus. *Meteorit. Planet. Sci.* **2003**, *38*, 1551–1578. https://doi.org/10.1111/j.1945-5100.2003.tb00001.x.
96. Gault, D.E.; Wedekind, J.A. Experimental studies of oblique impact. In Proceedings of the 9th Lunar and Planetary Science Conference, The Woodlands, Houston, TX, USA, 17 March 1978; Pergamon Press: New York, NY, 1978.
97. Zhang, X.; Xia, X.; Wang, Y. The origin of Messier crater rays and the model of oblique impact. *Prog. Geophys.* **2015**, *30*, 488–492. https://doi.org/10.6038/pg20150203.
98. Haruyama, J.; Hioki, K.; Shirao, M.; Morota, T.; Hiesinger, H.; van der Bogert, C.H.; Miyamoto, H.; Iwasaki, A.; Yokota, Y.; Ohtake, M.; et al. Possible lunar lava tube skylight observed by SELENE cameras. *Geophys. Res. Lett.* **2009**, *36*. https://doi.org/10.1029/2009GL040635.
99. Wagner, R.V.; Robinson, M.S. Distribution, formation mechanisms, and significance of lunar pits. *Icarus* **2014**, *237*, 52–60. https://doi.org/10.1016/j.icarus.2014.04.002.
100. Robinson, M.S.; Ashley, J.W.; Boyd, A.K.; Wagner, R.V.; Speyerer, E.J.; Ray Hawke, B.; Hiesinger, H.; van der Bogert, C.H. Confirmation of sublunarean voids and thin layering in mare deposits. *Planet. Space Sci.* **2012**, *69*, 18–27. https://doi.org/10.1016/j.pss.2012.05.008.

101. Kaku, T.; Haruyama, J.; Miyake, W.; Kumamoto, A.; Ishiyama, K.; Nishibori, T.; Yamamoto, K.; Crites, S.T.; Michikami, T.; Yokota, Y.; et al. Detection of Intact Lava Tubes at Marius Hills on the Moon by SELENE (Kaguya) Lunar Radar Sounder. *Geophys. Res. Lett.* **2017**, *44*, 10155–10161. https://doi.org/10.1002/2017GL074998.
102. Chappaz, L.; Sood, R.; Melosh, H.J.; Howell, K.C.; Blair, D.M.; Milbury, C.; Zuber, M.T. Evidence of large empty lava tubes on the Moon using GRAIL gravity. *Geophys. Res. Lett.* **2017**, *44*, 105–112. https://doi.org/10.1002/2016GL071588.
103. Hood, L.L.; Schubert, G. Lunar Magnetic Anomalies and Surface Optical Properties. *Science* **1980**, *208*, 49–51. https://doi.org/10.1126/science.208.4439.49.
104. Neish, C.D.; Blewett, D.T.; Bussey, D.; Lawrence, S.J.; Mechtley, M.; Thomson, B.J. The surficial nature of lunar swirls as revealed by the Mini-RF instrument. *Icarus* **2011**, *215*, 186–196. https://doi.org/10.1016/j.icarus.2011.06.037.
105. Glotch, T.D.; Bandfield, J.L.; Lucey, P.G.; Hayne, P.O.; Greenhagen, B.T.; Arnold, J.A.; Ghent, R.R.; Paige, D.A. Formation of lunar swirls by magnetic field standoff of the solar wind. *Nat. Commun.* **2015**, *6*, 6189. https://doi.org/10.1038/ncomms7189.
106. Li, S.; Garrick-Bethell, I. Surface Water at Lunar Magnetic Anomalies. *Geophys. Res. Lett.* **2019**, *46*, 14318–14327. https://doi.org/10.1029/2019GL084890.
107. Schultz, P.H.; Srnka, L.J. Cometary collisions on the Moon and Mercury. *Nature* **1980**, *284*, 22–26. https://doi.org/10.1038/284022a0.
108. Pinet, P.C.; Shevchenko, V.V.; Chevrel, S.D.; Daydou, Y.; Rosemberg, C. Local and regional lunar regolith characteristics at Reiner Gamma Formation: Optical and spectroscopic properties from Clementine and Earth-based data. *J. Geophys. Res.* **2000**, *105*, 9457–9475. https://doi.org/10.1029/1999JE001086.
109. Syal, M.B.; Schultz, P.H. Cometary impact effects at the Moon: Implications for lunar swirl formation. *Icarus* **2015**, *257*, 194–206. https://doi.org/10.1016/j.icarus.2015.05.005.
110. Garrick-Bethell, I.; Head, J.W.; Pieters, C.M. Spectral properties, magnetic fields, and dust transport at lunar swirls. *Icarus* **2011**, *212*, 480–492. https://doi.org/10.1016/j.icarus.2010.11.036.
111. Managadze, G.G.; Cherepin, V.T.; Shkuratov, Y.G.; Kolesnik, V.N.; Chumikov, A.E. Simulating OH/H2O formation by solar wind at the lunar surface. *Icarus* **2011**, *215*, 449–451. https://doi.org/10.1016/j.icarus.2011.06.025.
112. Chaussidon, M. Lunar water from the solar wind. *Nat. Geosci.* **2012**, *5*, 766–767. https://doi.org/10.1038/ngeo1616.
113. Green, R.O.; Pieters, C.; Mouroulis, P.; Eastwood, M.; Boardman, J.; Glavich, T.; Isaacson, P.; Annadurai, M.; Besse, S.; Barr, D.; et al. The Moon Mineralogy Mapper (M3) imaging spectrometer for lunar science: Instrument description, calibration, on-orbit measurements, science data calibration and on-orbit validation. *J. Geophys. Res.* **2011**, *116*, 367. https://doi.org/10.1029/2011JE003797.
114. Tsunakawa, H.; Takahashi, F.; Shimizu, H.; Shibuya, H.; Matsushima, M. Surface vector mapping of magnetic anomalies over the Moon using Kaguya and Lunar Prospector observations. *J. Geophys. Res.* **2015**, *120*, 1160–1185. https://doi.org/10.1002/2014JE004785.
115. Benaroya, H.; Bernold, L.; Chua, K.M. Engineering, Design and Construction of Lunar Bases. *J. Aerosp. Eng.* **2002**, *15*, 33–45. https://doi.org/10.1061/(ASCE)0893-1321(2002)15:2(33).
116. Daga, A.W.; Daga, M.A.; Wendel, W.R. A Preliminary Assessment of the Potential of Lava Tube-Situated Lunar Base Architecture. In *Engineering, Construction, and Operations in Space II*; ASCE: Reston, VI, USA, 1990; pp. 568–577.
117. Horvath, T.; Hayne, P.O.; Paige, D.A. Thermal Environments and Illumination in Lunar Pits and Lava Tubes. In *AGU Fall Meeting Abstracts 2019*; AGU: Washington, DC, USA, 2019; p. P31C-3454.
118. Haruyama, J.; Sawai, S.; Mizuno, T.; Yoshimitsu, T.; Fukuda, S.; Nakatani, I. Exploration of Lunar Holes, Possible Skylights of Underlying Lava Tubes, by Smart Lander for Investigating Moon (SLIM). *Trans. JSASS Aerosp. Tech. Jpn.* **2012**, *10*, Pk_7–Pk_10. https://doi.org/10.2322/tastj.10.Pk_7.
119. De Angelis, G.; Wilson, J.W.; Clowdsley, M.S.; Nealy, J.E.; Humes, D.H.; Clem, J.M. Lunar lava tube radiation safety analysis. *J. Radiat. Res.* **2002**, *43*, S41–S45. https://doi.org/10.1269/jrr.43.s41.
120. Haruyama, J.; Morota, T.; Kobayashi, S.; Sawai, S.; Lucey, P.G.; Shirao, M.; Nishino, M.N. Lunar Holes and Lava Tubes as Resources for Lunar Science and Exploration. In *Moon*: *Prospective Energy and Material Resources*; Badescu, V., Ed.; Springer: Berlin/Heidelberg, Germany, 2012; pp. 139–163, ISBN 978-3-642-27968-3.
121. Cadogan, D.; Stein, J.; Grahne, M. Inflatable composite habitat structures for lunar and mars exploration. *Acta Astronaut.* **1999**, *44*, 399–406. https://doi.org/10.1016/S0094-5765(99)00103-4.
122. Katzer, J.; Suchocki, C.; Błaszczak-Bąk, W.; Zarzycki, P.K.; Damięcka-Suchocka, M. Reliability and effectiveness of laser scanners in future construction efforts on the Moon and Mars. *Autom. Constr.* **2021**, *132*, 103979. https://doi.org/10.1016/j.autcon.2021.103979.
123. Draper, D.S.; Lawrence, S.J.; Klima, R.S.; Denevi, B.W.; van der Bogert, C.H.; Elardo, S.M.; Hiesinger, H.H. The Inner Solar System Chronology (ISOCHRON) Lunar Sample Return Mission Concept: Revealing Two Billion Years of History. *Planet. Sci. J.* **2021**, *2*, 79. https://doi.org/10.3847/PSJ/abe419.
124. Robbins, S.J. New crater calibrations for the lunar crater-age chronology. *Earth Planet. Sci. Lett.* **2014**, *403*, 188–198. https://doi.org/10.1016/j.epsl.2014.06.038.
125. Neukum, G.; Ivanov, B.A.; Hartmann, W.K. Cratering Records in the Inner Solar System in Relation to the Lunar Reference System. In *Chronology and Evolution of Mars*; Kallenbach, R., Geiss, J., Hartmann, W.K., Eds.; Springer: Dordrecht, The Netherlands, 2001; pp. 55–86, ISBN 978-94-017-1035-0.

126. Marchi, S.; Mottola, S.; Cremonese, G.; Massironi, M.; Martellato, E. A new chronology for the Moon and Mercury. *Astron. J.* **2009**, *137*, 4936–4948. https://doi.org/10.1088/0004-6256/137/6/4936.
127. Hartmann, W.K.; Quantin, C.; Mangold, N. Possible long-term decline in impact rates. *Icarus* **2007**, *186*, 11–23. https://doi.org/10.1016/j.icarus.2006.09.009.
128. van der Bogert, C.H.; Hiesinger, H. Which Samples are Needed for Improved Calibration of the Lunar Cratering Chronology? In Proceedings of the 51st Lunar and Planetary Science Conference, Virtual Event, 15–19 March 2021; p. 2088.
129. Williams, J.-P.; van der Bogert, C.H.; Pathare, A.V.; Michael, G.G.; Kirchoff, M.R.; Hiesinger, H. Dating very young planetary surfaces from crater statistics: A review of issues and challenges. *Meteorit. Planet. Sci.* **2018**, *53*, 554–582. https://doi.org/10.1111/maps.12924.
130. Che, X.; Nemchin, A.; Liu, D.; Long, T.; Wang, C.; Norman, M.D.; Joy, K.H.; Tartese, R.; Head, J.; Jolliff, B.; et al. Age and composition of young basalts on the Moon, measured from samples returned by Chang'e-5. *Science* **2021**, *374*, 887–890. https://doi.org/10.1126/science.abl7957.
131. Li, Q.-L.; Zhou, Q.; Liu, Y.; Xiao, Z.; Lin, Y.; Li, J.-H.; Ma, H.-X.; Tang, G.-Q.; Guo, S.; Tang, X.; et al. Two billion-year-old volcanism on the Moon from Chang'E-5 basalts. *Nature* **2021**, *600*, 54–58. https://doi.org/10.1038/s41586-021-04100-2.
132. Stevenson, D.J. Origin of the Moon-The Collision Hypothesis. *Annu. Rev. Earth Planet. Sci.* **1987**, *15*, 271–315. https://doi.org/10.1146/annurev.ea.15.050187.001415.
133. Spohn, T. The Longevity of Lunar Volcanism: Implications of Thermal Evolution Calculations with 2D and 3D Mantle Convection Models. *Icarus* **2001**, *149*, 54–65. https://doi.org/10.1006/icar.2000.6514.
134. Schultz, P.H.; Spudis, P.D. Beginning and end of lunar mare volcanism. *Nature* **1983**, *302*, 233–236. https://doi.org/10.1038/302233a0.
135. Haskin, L.A.; Gillis, J.J.; Korotev, R.L.; Jolliff, B.L. The materials of the lunar Procellarum KREEP Terrane: A synthesis of data from geomorphological mapping, remote sensing, and sample analyses. *J. Geophys. Res.* **2000**, *105*, 20403–20415. https://doi.org/10.1029/1999JE001128.
136. Jolliff, B.L.; Gillis, J.J.; Haskin, L.A.; Korotev, R.L.; Wieczorek, M.A. Major lunar crustal terranes: Surface expressions and crust-mantle origins. *J. Geophys. Res.* **2000**, *105*, 4197–4216. https://doi.org/10.1029/1999JE001103.
137. Wieczorek, M.A.; Phillips, R.J. The "Procellarum KREEP Terrane": Implications for mare volcanism and lunar evolution. *J. Geophys. Res.* **2000**, *105*, 20417–20430. https://doi.org/10.1029/1999JE001092.
138. Tian, H.-C.; Wang, H.; Chen, Y.; Yang, W.; Zhou, Q.; Zhang, C.; Lin, H.-L.; Huang, C.; Wu, S.-T.; Jia, L.-H.; et al. Non-KREEP origin for Chang'E-5 basalts in the Procellarum KREEP Terrane. *Nature* **2021**, *600*, 59–63. https://doi.org/10.1038/s41586-021-04119-5.
139. Li, C.; Hu, H.; Yang, M.-F.; Pei, Z.-Y.; Zhou, Q.; Ren, X.; Liu, B.; Liu, D.; Zeng, X.; Zhang, G.; et al. Characteristics of the lunar samples returned by Chang'E-5 mission. *Natl. Sci. Rev.* **2021**, *9*, nwab188. https://doi.org/10.1093/nsr/nwab188.
140. Hu, S.; He, H.; Ji, J.; Lin, Y.; Hui, H.; Anand, M.; Tartèse, R.; Yan, Y.; Hao, J.; Li, R.; et al. A dry lunar mantle reservoir for young mare basalts of Chang'E-5. *Nature* **2021**, *600*, 49–53. https://doi.org/10.1038/s41586-021-04107-9.
141. Delano, J.W. Pristine lunar glasses: Criteria, data, and implications. *J. Geophys. Res.* **1986**, *91*, 201–213. https://doi.org/10.1029/JB091iB04p0D201.
142. Shearer, C.; Papike, J. Basaltic magmatism on the Moon: A perspective from volcanic picritic glass beads. *Geochim. Cosmochim. Acta* **1993**, *57*, 4785–4812. https://doi.org/10.1016/0016-7037(93)90200-G.
143. Saal, A.E.; Hauri, E.H.; Cascio, M.L.; van Orman, J.A.; Rutherford, M.C.; Cooper, R.F. Volatile content of lunar volcanic glasses and the presence of water in the Moon's interior. *Nature* **2008**, *454*, 192–195. https://doi.org/10.1038/nature07047.
144. Saal, A.E.; Hauri, E.H.; van Orman, J.A.; Rutherford, M.J. Hydrogen Isotopes in Lunar Volcanic Glasses and Melt Inclusions Reveal a Carbonaceous Chondrite Heritage. *Science* **2013**, *340*, 1317–1320. https://doi.org/10.1126/science.1235142.
145. Hauri, E.H.; Weinreich, T.; Saal, A.E.; Rutherford, M.C.; van Orman, J.A. High Pre-Eruptive Water Contents Preserved in Lunar Melt Inclusions. *Science* **2011**, *333*, 213–215. https://doi.org/10.1126/science.1204626.
146. Hauri, E.H.; Saal, A.E.; Rutherford, M.J.; van Orman, J.A. Water in the Moon's interior: Truth and consequences. *Earth Planet. Sci. Lett.* **2015**, *409*, 252–264. https://doi.org/10.1016/j.epsl.2014.10.053.
147. Milliken, R.E.; Li, S. Remote detection of widespread indigenous water in lunar pyroclastic deposits. *Nat. Geosci.* **2017**, *10*, 561–565. https://doi.org/10.1038/ngeo2993.
148. Trang, D.; Tonkham, T.; Filiberto, J.; Li, S.; Lemelin, M.; Elder, C.M. Eruption characteristics of lunar localized pyroclastic deposits as evidenced by remotely sensed water, mineralogy, and regolith. *Icarus* **2022**, *375*, 114837. https://doi.org/10.1016/j.icarus.2021.114837.
149. Robinson, M.; Elliott, J. Intrepid Planetary Mission Concept Study Report. 2020. Available online: https://science.nasa.gov/files/science-red/s3fs-public/atoms/files/Lunar%20INTREPID.pdf (accessed on 22 September 2020).
150. Haruyama, J.; Matsunaga, T.; Ohtake, M.; Morota, T.; Honda, C.; Yokota, Y.; Torii, M.; Ogawa, Y. Global lunar-surface mapping experiment using the Lunar Imager/Spectrometer on SELENE. *Earth Planets Space* **2008**, *60*, 243–255. https://doi.org/10.1186/BF03352788.

151. Li, M.; Tian, D.-B.; Bai, Y.; Wang, Z.-H.; Yu, Q.; Li, Y. Simulation test on lunar dust raising by lunar rover wheel. In *Design, Manufacturing and Mechatronics, Proceedings of the 2015 International Conference on Design, Manufacturing, and Mechatronics (ICDMM2015)*, Wuhan, China, 17–18 April 2015; Shahhosseini, A.M., Ed.; World Scientific: Hackensack, NJ, USA, 2016; pp. 35–40. ISBN 978-981-4730-50-1.
152. Li, M.; Wang, H.; Tian, D.; Tong, J.; Lv, Z.; Li, Y. Discrete Element Simulation of lunar dust suspension caused by lunar rover wheel. In Proceedings of the International Conference on Transportation, Mechanical, and Electrical Engineering (TMEE), Changchun, China, 16–18 December 2011; IEEE: New York, NY, USA, 2011; pp. 316–319. ISBN 978-1-4577-1701-7.